JOURNAL OF THE ATMOSPHERIC SCIENCES

Atmospheric gravity wave ray tracing: Ordinary and extraordinary waves (Version submitted 6 October 2017: Draft: December 28, 2017, 9:38am)

R. MICHAEL JONES* AND ALFRED J. BEDARD JR.

Cooperative Institute for Research in Environmental Sciences, University of Colorado, Boulder, Colorado

ABSTRACT

Calculation of internal gravity-wave ray paths in the atmosphere using a general three-dimensional ray tracing computer program is discussed. Including the effects of wind on the propagation of gravity waves complicates the calculation of the ray paths because not only must one specify frequency and direction of propagation (wave-normal direction), one must also choose among four kinds of waves. Two of these waves (designated here as "ordinary waves," in analogy with electromagnetic wave propagation) correspond to the usual acoustic-gravity waves in the absence of winds, while the other two have wavenumbers that approach infinity as the wind speed approaches zero. These latter two waves (designated here as "extraordinary waves") correspond to asymptotic gravity waves. Comparison with previously published examples of ray-path calculations of gravity waves shows that those previous examples were actually extraordinary waves, but their significance was not recognized at that time. Extraordinary waves may be important in the dissipation of gravity-wave energy.

1. Introduction

Gravity waves are ubiquitous in the atmosphere because they are generated by earthquakes, tsunamis, volcanic eruptions, severe storms, and nuclear explosions, in addition to less spectacular mechanisms (e.g. situations where the Richardson number is less than 1/4). See, for example, the work by Stenflo (1986, 1987, 1991, 1996); Stenflo and Stepanyants (1995); Jurén and Stenflo (1973) and the review by Fritts and Alexander (2003, 2012). Section 2 reviews the broad range of atmospheric gravity wave generation mechanisms and their areas of practical impacts.

Atmospheric gravity waves can be detected directly using arrays of pressure sensors (e.g. Liu et al. 1982; Bedard 1984; Bedard et al. 2004; Bedard 1982) or can be detected indirectly by using Lidar measurements of temperature profiles (e.g. Chen et al. 2013, 2016) or by measuring the effects of gravity waves in the ionosphere (Nekrasov et al. 1995; Rolland et al. 2010; Makela et al. 2011; Hickey et al. 2009; Artru et al. 2005) or troposphere (Arai et al. 2011; Hickey et al. 2009). In the case of gravity wave propagation to the ionosphere, it is necessary to consider the effect of the Earth's magnetic field (Nekrasov et al. 1995; Pokhotelov et al. 1996; Nekrasov et al. 1992; Pokhotelov et al. 1994; Chmyrev et al. 1991; Pokhotelov et al. 1998; Streltsov et al. 1990) and to use a dispersion relation for magneto-acoustic-gravity waves (Ostrovsky 2008; Jones et al. 2017).

Determining the sources of atmospheric gravity waves and understanding how atmospheric gravity waves are generated by their sources is an area of active research. Using ray tracing to help interpret the propagation of gravity waves helps in that endeavor and in part has motivated our work. For example, we are using ray tracing to help interpret the gravity waves observed by Lidar measurements of temperature profiles in Antarctica (Chen et al. 2013, 2016; Zhao et al. 2017).

Section 3 discusses ray tracing, including giving the dispersion relation we used in our ray path calculations. Section 4 shows propagation effects of the Acoustic cutoff frequency and the Brunt-Väisälä frequency. Section 5 shows how the ray tracing program calculates the magnitude of the wave vector to initialize the calculation of a ray path. In the presence of wind, there are two types of waves, which we refer to as "ordinary" and "extraordinary." Section 6 shows dispersion-relation diagrams for gravity waves with and without wind. The dispersion-relation diagrams for the extraordinary waves are very different from those for the ordinary waves. Section 7 shows the effect of including wind on the propagation of gravity waves. Extraordinary wave ray paths are very different from those for ordinary waves. Section 8 compares our ray path calculations and analysis with gravity-wave ray-

*Corresponding author address: Cooperative Institute for Research in Environmental Sciences, University of Colorado, Boulder, Colorado 80309-0216/U.S.A.

E-mail: Michael.Jones@Colorado.edu

path calculations of others. We show that some previously published examples of gravity-wave ray paths are actually extraordinary waves. Section 9 discusses meteorological applications of a gravity wave ray tracing program. Section 10 gives some concluding remarks.

2. Impact areas of atmospheric gravity waves

The areas listed below, with examples, reflect the broad impacts of atmospheric gravity waves in terms of being generated by a rich variety of phenomena, initiating geophysical events, and transferring energy, permitting interactions between the lithosphere, atmospheric layers and the ionosphere. In addition, gravity waves can provide information for warning of the existence of potential hazards (e.g. aircraft turbulence, tsunamis). The lower atmospheric boundary layer involves interacting wind shears, thermal plumes, turbulence, and gravity waves- combining in complex interactions. At times lower level wind shear, instabilities, and gravity waves can produce the erosion of ground based inversions. In other situations thermal plumes can dominate the boundary layer. During the nocturnal boundary layer gravity waves can control the near surface dynamics.

In addition, many major field experiments have measured the properties of atmospheric gravity waves using combinations of remotes sensors and aircraft probes. The DEEPWAVE program (Fritts et al. 2016) is a recent example of an extensive effort to define gravity wave sources and effects in the lower and middle atmosphere. Gravity wave ray trace programs could have a role in helping to guide aircraft and remote sensing measurements. Also, there exist large regional scale efforts to apply high density surface arrays e.g. the USARRAY (Tytell et al. 2016) and also global arrays designed as part of an International Monitoring System (IMS) for monitoring nuclear explosions (Christie and Campus 2009). Both these arrays have the ability to measure atmospheric gravity wave induced pressure changes. Gravity wave ray tracing can assist in the interpretation of surface array pressure measurements that can provide azimuth and phase speed information.

a. Examples of Gravity Wave Generation Processes

- Convection (Deardorff et al. 1969; Vadas and Fritts 2009; Alexander 1996)
- Severe weather (Bowman and Bedard 1971; Balachandran 1980; Curry and Murty 1974; Nicholls and Pielke 1994a,b)
- Large explosions, volcanoes (ReVelle 2009)
- Mountain waves (Schoeberl 1985)
- Terrain forcing (Nappo 2002)
- Sudden stratospheric warming (Gerrard et al. 2011)
- Fronts (Wrasse et al. 2006; Lin and Zhang 2008)
- Jets (Suzuki et al. 2013)
- Sea wave forcing (Vadas et al. 2015)
- Geomagnetic activity (Chimonas and Hines 1970; Testud 1970)
- Solar eclipse (Chimonas and Hines 1970)

b. Examples of gravity waves in the atmospheric boundary layer

- Gravity waves associated with wind shear induced instabilities (Pramitha et al. 2015)
- Gravity waves associated with temperature inversions (Williams et al. 2002; Bedard et al. 1981; Cunningham and Bedard 1993)
- Gravity waves associated with the atmospheric boundary layer (Einaudi et al. 1989)
- Gravity waves and boundary layer rolls (Li et al. 2013)
- Gravity waves associated with convective plumes (Vadas and Fritts 2009)

c. Examples of gravity wave initiation of geophysical events

- Severe storm initiation (Uccelini 1975)
- Sea surface excitation (Šepić et al. 2015)
- Aircraft turbulence (Bedard et al. 1986)
- Modulation of gust surges (Beluši'c et al. 2004)

d. Examples of gravity wave energy transfer

- Atmospheric general circulation models (Lott and Millet 2009)
- Convectively generated gravity waves (Alexander 1996)

e. Examples of possible gravity wave applications for hazard warning and characterization

- Earthquakes (Mikumo and Watada 2009)
- Tsunamis (Mikumo and Watada 2009)
- Meterological Tsunamis (Šepić et al. 2015)
- Earthquake precursors (Lognonné 2009)
- Hurricanes (Hung and Kuo 1978; Hung and Smith 1978)

- Tornadic storms (Hung et al. 1979)
- Aircraft turbulence (Bedard et al. 1986)

3. Ray tracing

Ray tracing is a practical method for calculating the ray-theory or WKB approximation for the propagation of waves in a specified medium. Jones (1996) reviews the conditions for the validity of ray theory and the WKB approximation. Simple tests based on the wavelength of the waves are often inaccurate estimates for the validity of the WKB approximation. The propagation of gravity waves in the atmosphere can be calculated using a ray tracing program based on Hamilton's equations if the dispersion relation is used as the Hamiltonian. The usual barotropic dispersion relation for acoustic-gravity waves (which includes both acoustic and gravity waves) is (Eckart 1960, eq. (51-2), p. 125)(Gossard and Hooke 1975, eq. (23-7), p. 112)

$$\left(\omega_i^2 - 4\Omega_z^2\right)\left(k_z^2 + \mathbf{k}_A^2 - \frac{\omega_i^2}{C^2}\right) - \left(k_x^2 + k_y^2\right)\left(N^2 - \omega_i^2\right) = 0\,, \tag{1}$$

where[1]

$$k_A^2 = \frac{\omega_a^2}{C^2} = \frac{N^2}{C^2} + \Gamma^2 = \frac{1}{4H^2}\,, \tag{2}$$

H is the density scale height, N is the Brunt-Väisälä frequency, C is sound speed, ω_a is the acoustic cutoff frequency, $\Gamma \equiv \nabla\rho/(2\rho) - \nabla p/(\rho C^2)$ is the vector generalization of Eckart's coefficient,

$$\omega_i = \omega - \mathbf{k}\cdot\mathbf{U} = \omega - Ck\alpha \tag{3}$$

is the intrinsic frequency, where $\alpha \equiv \mathbf{k}\cdot\mathbf{U}/(Ck)$ is a dimensionless variable that gives the effect of the wind and wave-normal direction relative to the wind direction. ω is the wave frequency, $\mathbf{U}$ is the background wind velocity, $\mathbf{k}$ is the wavenumber, k_z is its vertical component, k_x and k_y are its horizontal components, and Ω_z is the vertical component of the Earth's angular velocity.

The dispersion relation (1) applies to any perfect fluid, such as the ocean or atmosphere. It applies to acoustic waves when the intrinsic frequency ω_i is above the acoustic cutoff frequency ω_a (where compressibility is the dominant restoring force), and to internal gravity waves when the intrinsic frequency ω_i is below the Brunt-Väisälä frequency N (where buoyancy from the Earth's gravitational field is the dominant restoring force).

There is a frequency gap between those two frequencies where all waves are evanescent. Because gravity waves and acoustic waves are separated by a frequency gap, it is always clear how to distinguish between an acoustic wave and a gravity wave. If the intrinsic frequency is above the acoustic cutoff frequency, then it is an acoustic wave. If the intrinsic frequency is below the Brunt-Väisälä frequency, then it is a gravity wave. This is true, even though gravity waves close to the Brunt-Väisälä frequency have some effect from compressibility as a restoring force and acoustic waves near the acoustic cutoff frequency have some effect from gravity as a restoring force. Nearly all of the waves considered here are gravity waves.

The dispersion relation (1) can be generalized to include baroclinicity (Jones 2001, 2012), vorticity, and rate-of-strain (Jones 2005, 2008a, 2006, 2008b). The calculations here use (1) for the dispersion relation, but neglect the Coriolis term $4\Omega_z^2$ from the Earth's rotation. The CIRES/NOAA acoustic-gravity wave ray tracing computer program used for these calculations is a general three-dimensional ray tracing program for calculating acoustic-gravity waves in the atmosphere (described in Bedard and Jones 2013; Jones and Bedard 2015) based on an earlier program HARPA for calculating the propagation of acoustic waves (Jones et al. 1986a,b; Georges et al. 1990). The ray tracing program calculates ray paths by integrating Hamilton's equations in Earth-centered spherical polar coordinates (Jones et al. 1986a, pp. 89-91).

Jones (1996) reviews the practical aspects of ray tracing, the WKB approximation, and the limits of geometrical optics to calculate wave propagation in the atmosphere. Although the WKB approximation was given its present name after 1926 (Wentzel 1926; Kramers 1926; Brillouin 1926), the method was discovered earlier (Liouville 1836, 1837a,b; Rayleigh (John William Strutt) 1912; Jeffreys 1923).

There are several ray tracing programs for calculating the propagation of acoustic and/or gravity waves (e.g., Preusse et al. 2008; Muraschko et al. 2013; Cowling et al. 1971; Broutman et al. 2004; Georges 1971; Vadas and Fritts 2009), including some programs that can calculate the effects of winds and dissipation.

There are several ways to initialize the ray parameters at the source, and all of the ways are equally valid, with it being purely a personal choice to choose one method over another. In the CIRES/NOAA ray tracing program, the user chooses the frequency and wave-normal direction, and the program uses the dispersion relation to determine the magnitude of the wave number k. Another possibility (possibly used by some ray tracing programs) is to choose the frequency and horizontal components of the wave number $\mathbf{k}$, and let the program determine the vertical component of the wavenumber from the dispersion relation. Still another possibility (Georges 1971) is to choose the wave-normal direction and the magnitude of the wave number k or total wavelength, and let the program determine the frequency from the dispersion relation. Section 8 shows that the ray paths Georges (1971) gave as examples are what we here classify as "extraordinary rays." The ordinary and extraordinary waves referred to here are not

[1] Equation (2) is consistent with $\mathbf{k}_A \equiv \nabla\rho/(2\rho)$, where ρ is density.

related to the "ordinary viscous waves" or the "extraordinary viscous waves" referred to by Volland (1969), Hickey and Cole (1987), or Ma (2016).

Jones (1969) points out a distinction between gravity waves that are propagating and gravity waves that are merely advected with the mean wind. Marks and Eckermann (1995) use their ray tracing program to compare turbulent diffusivity with scale-dependent infrared radiative damping. Preusse et al. (2009) compare their ray path calculations with measured global maps of gravity waves. Vadas and Fritts (2005) and Vadas (2007) include damping effects of kinematic viscosity and thermal diffusivity in the thermosphere in their ray path calculations. Vadas and Fritts (2009) use ray tracing to reconstruct the gravity wave field from convective plumes. Ding et al. (2003) includes viscosity and thermal conductivity in their ray path calculations. In addition, there is at least one gravity-wave resolving general circulation model (e.g. Sato et al. 2009). Although the dispersion relation for acoustic-gravity waves is not unique, the resulting WKB approximations from using the various dispersion relations will differ by an amount that is less than the error in the WKB approximations (Einaudi and Hines 1970; Weinberg 1962; Jones 2006). A ray will pass through a critical layer whenever the intrinsic frequency passes through zero. Booker and Bretherton (1967) show that waves passing through a critical level are attenuated by an amount that depends on the Richardson number. None of the ray paths in the examples presented here passed through a critical level.

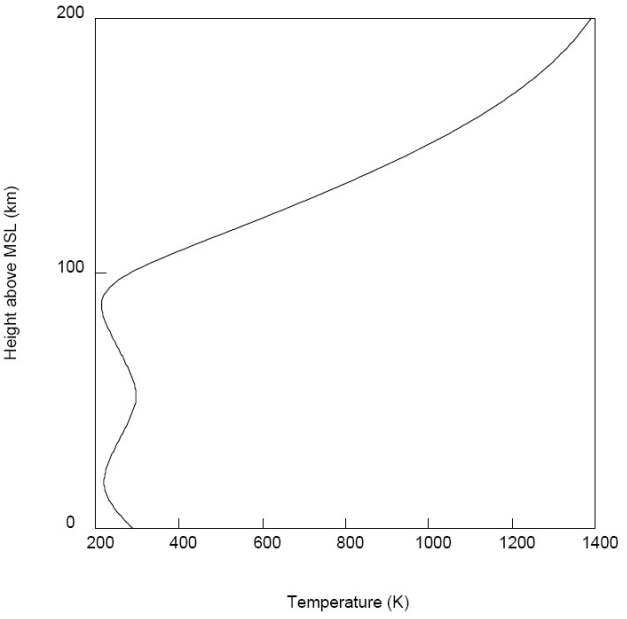

FIG. 1. 1962 Standard Atmosphere temperature profile used for all of the ray-path calculations presented here except for the calculations used for comparison with other work in figures 18 and 19. For these calculations, we had no longitude or latitude dependence of temperature.

4. Acoustic cutoff frequency and Brunt-Väisälä frequency

To illustrate the effect of the Acoustic cutoff frequency and Brunt-Väisälä frequency on propagation, we consider some examples.

The acoustic cutoff frequency profile and Brunt-Väisälä frequency profile are determined indirectly by the temperature profile, and directly by the pressure and density profiles. The latter are determined from the temperature profile through the equation of state and hydrostatic equilibrium.

As an example, we use the temperature profile in figure 1, but if we were making ray-path calculations to interpret measurements, we would use more realistic models such as those available from the NRLMSISE-00 Atmosphere Model (NRLMSISE-00, Community Coordinated Modeling Center 2016) or from measurements (e.g. Chu et al. 2011). For the temperature profile in figure 1, we get the acoustic cutoff frequency profile shown in figure 2, and the Brunt-Väisälä frequency profile shown in figure 3. Combining figures 2 and 3 illustrates the frequency gap shown in figure 4.

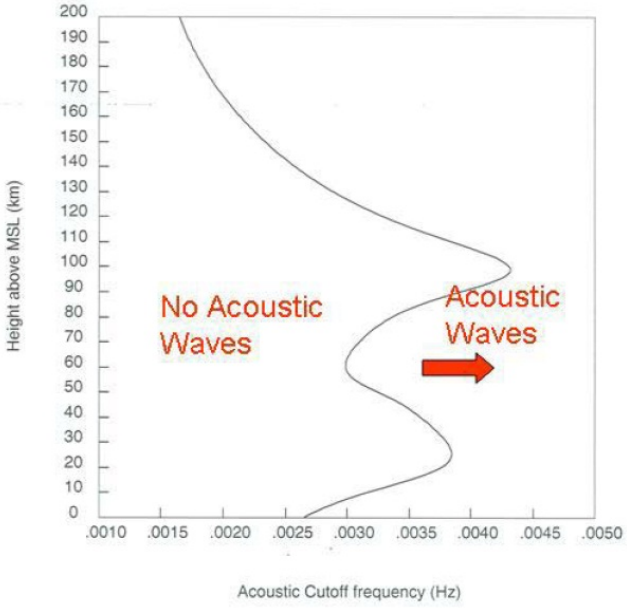

FIG. 2. Acoustic cutoff frequency profile from the temperature profile in figure 1. The acoustic cutoff frequency, ω_a, is calculated from $\omega_a = Ck_A = C|\nabla\rho|/(2\rho)$, where C is sound speed, and ρ is density (Jones 2005, 2006). (Color online)

Figure 4 shows that a frequency of 0.0032 Hz should be above the acoustic cutoff frequency at a height of 10 km. Confirming that, figure 5 shows that 0.0032 Hz waves

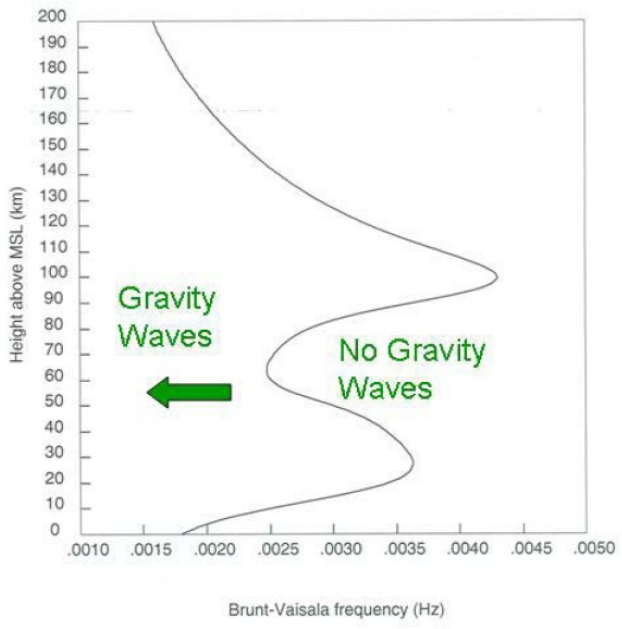

FIG. 3. Brunt-Väisälä frequency profile from the temperature profile in figure 1. The Brunt-Väisälä frequency, N, is calculated from $N^2 = \nabla\tilde{\rho}_{\rm pot}\cdot\tilde{\mathbf{g}}/\rho = (\nabla\rho - \nabla p/C^2)\cdot\tilde{\mathbf{g}}/\rho = [\rho\tilde{\mathbf{g}}/p - \nabla T/T + \nabla M/M - \nabla p/(\rho C^2)]\cdot\tilde{\mathbf{g}}$, where $\tilde{\rho}_{\rm pot}$ is local potential density, p is pressure, C is sound speed, $\tilde{\mathbf{g}} = \nabla p/\rho$ is the effective acceleration due to gravity, T is absolute temperature, and M is the molecular weight (Jones 2005, 2006). (Color online)

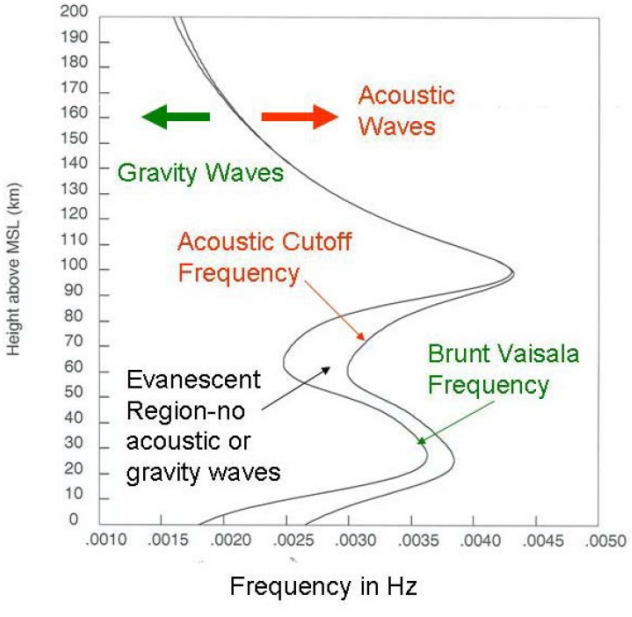

FIG. 4. Acoustic cutoff frequency and Brunt-Väisälä frequency profiles from the temperature profile in figure 1 (Color online)

launched at that height are reflected a little below 11 km. These are acoustic waves.

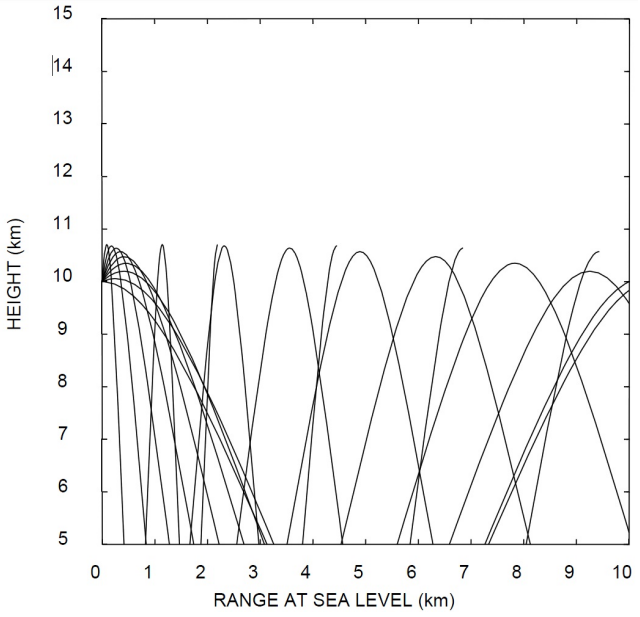

FIG. 5. Acoustic waves, f= 0.0032 Hz (above the acoustic cutoff frequency below about 10.8 km), source height is 10 km. The rays that stop at the top would reflect and return to the ground if we had continued the ray-path calculations.

Figure 4 also shows that a frequency of 0.00249 Hz should be below the Brunt-Väisälä frequency between the heights of about 10 and 60 km. Confirming that, figure 6 shows that a 0.00249 Hz wave is ducted between those two heights. This is a gravity wave. Only one gravity wave is shown here, because only a very narrow range of wave-normal directions give propagating waves at this frequency. Other wave-normal directions are evanescent at the source. We would see more waves propagate if we were to lower the frequency. The ray in figure 6 represents a guided gravity wave that is trapped in the 10-to-60-km height range.

Figure 7 gives an example of a lower frequency (0.00125 Hz) where gravity waves for a larger range of transmission directions can propagate. The source is at a height of 5 km. The elevation angle of transmission is stepped from 10° degrees to 90° in steps of 5°, but waves for elevation angles of transmission of 55° and higher are evanescent. That the wavelengths at the source of the waves in figure 7 are large does not necessarily indicate either a breakdown in ray theory or large errors in the WKB approximation. Estimating the errors in the WKB approximation involves locating turning points of the rays, calculating the size of the Airy regions around the turning points, recognizing possible overlaps of Airy regions, and determing if there are any singularities close to turning points (Jones 1996). Figure 7 has empty space on the left because we chose to plot figures 7, 12, and 13 on the same scale for easy comparison.

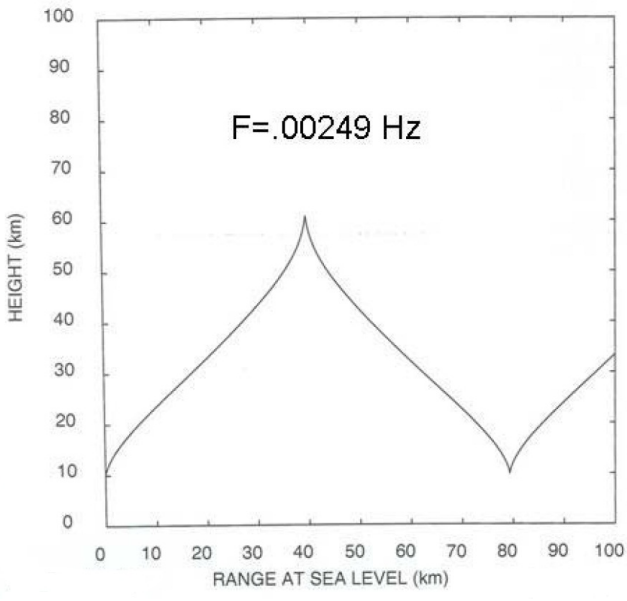

FIG. 6. Gravity wave, f= 0.00249 Hz, below the Brunt-Väisälä frequency between 10 and 60 km, source height is 10 km. The vertical component of the wave-normal vector is zero at the reflection height. Notice the similarity of the cusps in the ray path with the cusps in the ray paths in Figure 80 of page 336 in Lighthill's book (Lighthill 1978). Lighthill refers to the reflection height as a "critical level," but uses the terminology "special type of critical level" to refer to what is ususlly referred to as a "critical level" (i.e., where the intrinsic frequency, the frequency which would be observed by someone moving with the wind, becomes zero).

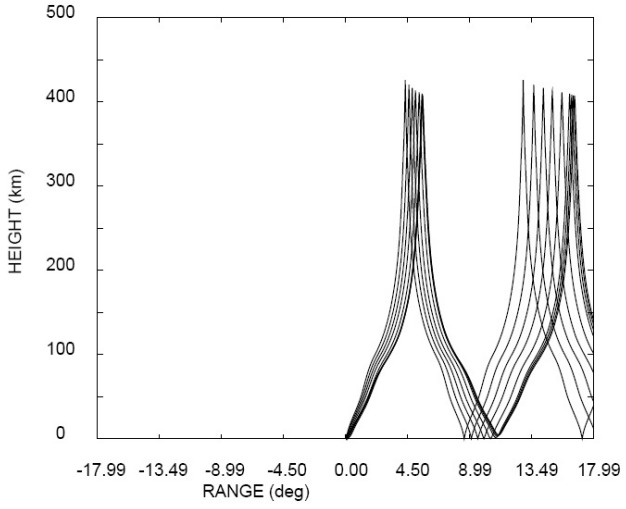

FIG. 7. Gravity waves without wind, f= 0.00125 Hz. Elevation angle of transmission varies from 10° to 50° in steps of 5°. The waves are evanescent for elevation angles of transmission equal to 55° and above. The source height is 5 km. The distance between tick marks on the horizontal axis is 500 km. The 10° elevation-angle ray reaches an apogee of 407 km at a range of 622 km in 2.35 hours, and has a wavelength at the source of 161 km. The 50° elevation-angle ray reaches an apogee of 425 km at a range of 482 km in 5.46 hours, and has a wavelength at the source of 44 km.

5. Initializing a ray path calculation for a specified frequency and direction of propagation

In the CIRES/NOAA ray tracing program, the user chooses the frequency and wave-normal direction, and the program uses the dispersion relation to determine the magnitude of the wave number ($k = 2\pi/\lambda$) to initialize the ray at the source. In the absence of wind, the dispersion relation (1) gives a simple formula to determine the magnitude of the wave-number. When there is wind, however, the dispersion relation (1) gives a quartic equation to determine the magnitude of the wave-number. It is then necessary to decide which of the four roots of that quartic equation will give the desired ray path. The following discussion addresses that problem, and in the process, finds it useful to differentiate between two kinds of waves, which we refer to as "ordinary" and "extraordinary."

In ray tracing programs that use other methods for initializing a ray-path calculation, it is possible that a quartic equation is not encountered in the initializing process, so that the distinction between the two kinds of waves that we characterize as ordinary and extraordinary was not previously discovered. For example, if the frequency and the horizontal components of the wavenumber are chosen, it is not necessary to solve a quartic equation to initialize the ray path calculation. For pure gravity waves, if the wave-normal direction and the magnitude of the wavenumber are chosen, it is also not necessary to solve a quartic equation to initialize the ray path calculation, but for acoustic-gravity waves, it would still be necessary to solve a quartic equation. However, the existence of ordinary and extraordinary gravity waves does not depend on the method of initializing a ray-path calculation, as can be seen from the dispersion-relation diagrams in section 6.

Examination of the dispersion relation (1) shows that the wavenumber for acoustic waves varies from zero at the acoustic cutoff frequency to infinity at infinite frequency in the absence of wind. Including wind complicates the situation, as is demonstrated later.

Similarly, the wavenumber for gravity waves varies from a small value to infinity in the absence of wind. Including wind (as will be shown later) separates solutions of the dispersion relation into separate branches, where the wavenumber can be infinite in some branches, but not others.

Substituting (3) into (1) and rearranging terms gives a quartic equation to determine k when given the wave frequency ω and the wave-normal direction.

$$\begin{aligned}&(1-\alpha^2)\alpha^2(Ck)^4 - 2\omega\alpha(1-2\alpha^2)(Ck)^3\\ &+\left[(1-6\alpha^2)\omega^2 + (\omega_a\alpha)^2 - \left(k_\perp^2/k^2\right)N^2\right](Ck)^2\\ &+2\omega\alpha(2\omega^2-\omega_a^2)Ck - \omega^2(\omega^2-\omega_a^2) = 0\,, \qquad (4)\end{aligned}$$

where we have neglected the Coriolis term Ω_z, $k_\perp^2 \equiv k_x^2 + k_y^2$ is the square of the horizontal component of the wave

vector, we have used $k^2 = k_z^2 + k_\perp^2$, $\omega_a = Ck_A$ is the acoustic cutoff frequency, and notice that the quantity $k_\perp^2/k^2$ depends only on the wave-normal direction. Although by definition, k is positive, (4) can have negative roots. The negative roots are referred to here as extraneous roots.

When calculating ray paths with the CIRES/NOAA ray tracing program, the height, longitude, and latitude of the source, the wave frequency, and the wave-normal direction are specified as input parameters. That determines the coefficients for the quartic equation (4). In addition, we specify in the input data whether we want to calculate an ordinary ray, an extraordinary ray, or one of the four quartic roots as root 1, 2, 3, or 4. The program then solves the quartic equation to find the four solutions of (4), and chooses (based on the input data) one of those four solutions to begin the ray path calculations. Since the wave-normal direction at the source is known, choosing one of the four values for k allows all three components of the wave vector $\mathbf{k}$ to be determined at the source. From that point on, numerically integrating Hamilton's equations gives the ray location and all three components of the wave vector $\mathbf{k}$ along the ray.

To give insight into the propagation, it is useful to understand the meaning of the four roots of the quartic. Wind speed is normally much smaller than the sound speed C, so that the dimensionless parameter α is also small. By seeing the behavior of the quartic equation as α approaches zero, we can understand the significance of the four roots. More detail is given in subsections a, b, and c.

a. Ordinary waves

All of the ray path calculations presented here use the full dispersion relation (1) (but neglecting the Coriolis term), which is then equivalent to (4). However, we here make some approximations to (4) to give insight into the nature of the ordinary and extraordinary waves.

We define an ordinary wave as the wave that would exist in the absence of wind. Therefore, to find approximate roots of (4) for the ordinary wave for small wind speed, we neglect terms in (4) that would not contribute to approximate solutions of (4) to first order. This gives a quadratic equation to give an approximate formula for k:

$$\begin{aligned}&\left[\omega^2 - \tfrac{k_\perp^2}{k^2}N^2\left(1+\tfrac{2Ck\alpha}{\omega}\right)\right](Ck)^2\\ &+2\omega^3\alpha Ck - \omega^2(\omega^2-\omega_a^2) = 0\,. \end{aligned} \tag{5}$$

An approximate solution of (5) to lowest order in α is

$$k \approx \frac{\omega}{C}\sqrt{\frac{\omega^2-\omega_a^2}{\omega^2-\frac{k_\perp^2}{k^2}N^2}} - \frac{\omega\alpha}{C}\frac{\omega^4 - \frac{k_\perp^2}{k^2}N^2\left(2\omega^2-\omega_a^2\right)}{\left(\omega^2-\frac{k_\perp^2}{k^2}N^2\right)^2}\,. \tag{6}$$

The CIRES/NOAA ray tracing program uses a numerical solution of the full quartic equation (4) to initialize a ray path calculation. The ray tracing program does not use the approximate formula (5) at all. Equation (5) is used here only to give insight into the propagation.

b. Extraordinary waves

The wavenumbers for the extraordinary wave are the large roots of the quartic equation (4). For these large roots, we look for solutions where $Ck\alpha$ is finite as α approaches zero. To first order in α, only the first three terms in (4) contribute to the solution for finite $Ck\alpha$. To show that, we divide (4) by $(Ck)^2$ to give

$$\begin{aligned}&(1-\alpha^2)(Ck\alpha)^2 - 2\omega(1-2\alpha^2)(Ck\alpha)\\ &+\left[(1-6\alpha^2)\omega^2 + (\omega_a\alpha)^2 - \left(k_\perp^2/k^2\right)N^2\right]\\ &+\alpha^2\left[2\omega(2\omega^2-\omega_a^2)Ck\alpha - \omega^2(\omega^2-\omega_a^2)\right]/(Ck\alpha)^2\\ &= 0\,. \end{aligned} \tag{7}$$

To find an approximate soulution of (7) for $Ck\alpha$ to first order in α, we neglect α^2 in (7) to give

$$(Ck\alpha)^2 - 2\omega(Ck\alpha) + \left[\omega^2 - \left(k_\perp^2/k^2\right)N^2\right] = 0\,. \tag{8}$$

Equation (8) has the solutions

$$k = \frac{\omega \pm (k_\perp/k)N}{C\alpha} = \frac{\omega \pm (k_\perp/k)N}{\mathbf{k}\cdot\mathbf{U}/k}\,. \tag{9}$$

Notice that these two roots approach infinity as the wind speed approaches zero.[2] (That is, the wavelength approaches zero as the wind speed approaches zero.) Notice that the intrinsic frequency for the solution given in (9) is given by $\omega_i = \mp(k_\perp/k)N$. That corresponds to an asymptotic gravity wave, which explains why there are no extraordinary acoustic waves. To find the next order approximate solution of (7) for small α, we could substitute the solution in (9) back into the last term in (7), and again solve the resulting quadratic equation in $Ck\alpha$.

The CIRES/NOAA ray tracing program uses a numerical solution of the full quartic equation (4) to initialize a ray path calculation. The ray tracing program does not use the approximate formula (9) at all. Equation (9) is used here only to give insight into the propagation.

For the case where the wind is horizontal, we can write (9) as

$$k = \frac{\omega \pm N(k_\perp/k)}{Uk_\perp/k}\,. \tag{10}$$

For downwind propagation at an angle θ from the horizontal, this gives

$$k = \frac{\omega \pm N\cos\theta}{U\cos\theta}\,, \tag{11}$$

[2]However, when the wind speed equals zero, these two roots disappear because (4) then changes from a quartic equation to a quadratic equation.

where the upper sign corresponds to the large extraordinary ray, and lower sign corresponds to the small extraordinary ray. For upwind propagation at an angle θ from the horizontal, this gives

$$k = \frac{\omega \mp N\cos\theta}{-U\cos\theta} \ , \tag{12}$$

where the upper sign corresponds to the small extraordinary ray, and lower sign corresponds to the extraneous large extraordinary ray.

c. Gravity waves

To give further insight into the properties of extraordinary waves, we consider the special case of gravity waves. To neglect acoustic waves, we neglect the third term in the second factor on the left side of (1). In addition, we neglect the Coriolis term. Neglecting those two terms, we substitute (3) into (1) and rearrange terms to give a quartic equation to determine k when given the wave frequency ω and the wave-normal direction. This gives

$$\begin{aligned} &\alpha^2(Ck)^4 - 2\alpha\omega(Ck)^3 \\ &- \left[\left(k_\perp^2/k^2\right)N^2 - \omega^2 - \alpha^2\omega_a^2\right](Ck)^2 \\ &-2\alpha\omega\omega_a^2 Ck + \omega^2\omega_a^2 = 0 \ . \end{aligned} \tag{13}$$

We can factor (13) to first order in α to give

$$\begin{aligned} &\left\{Ck - \frac{\omega\omega_a}{\sqrt{N^2k_\perp^2/k^2-\omega^2}} + \frac{\alpha\omega_a^2\omega N^2k_\perp^2/k^2}{\left(N^2k_\perp^2/k^2-\omega^2\right)^2}\right\}\times \\ &\left\{Ck + \frac{\omega\omega_a}{\sqrt{N^2k_\perp^2/k^2-\omega^2}} + \frac{\alpha\omega_a^2\omega N^2k_\perp^2/k^2}{\left(N^2k_\perp^2/k^2-\omega^2\right)^2}\right\}\times \\ &\{\alpha Ck - \omega - Nk_\perp/k\}\times\{\alpha Ck - \omega + Nk_\perp/k\} = \\ &\alpha^2(Ck)^4 - 2\alpha\omega(Ck)^3 - \left[\left(k_\perp^2/k^2\right)N^2 - \omega^2\right](Ck)^2 \\ &-2\alpha\omega\omega_a^2 Ck + \omega^2\omega_a^2 + \alpha^2 \text{ terms} + \alpha^3 \text{ terms} = 0 \ . \end{aligned} \tag{14}$$

For upwind propagation, the four factors in (14) are respectively the ordinary wave, the extraneous[3] ordinary wave solution, the small extraordinary wave, and the extraneous large extraordinary wave solution. For downwind propagation, the four factors in (14) are respectively the ordinary wave, the extraneous ordinary wave solution, the large extraordinary wave, and the small extraordinary wave.

6. Dispersion-relation diagrams

a. Without wind

A graphical representation of a dispersion relation is given by a dispersion-relation diagram. Figure 8 shows a dispersion-relation diagram without wind. It is a plot of vertical wavenumber on the vertical axis versus horizontal wavenumber on the horizontal axis for a constant frequency. Usually, in calculating a ray path, we choose the source location, the wave frequency, and the wave-normal direction to launch a ray. A straight line from the origin to the dispersion-relation curve gives an allowed wave-normal vector, in which the length of the line gives the wavenumber ($k = 2\pi/\lambda$, where λ is the wavelength), and the direction gives the normal to a wave front. The ray direction (which gives the direction of propagation of a pulse or wave packet) is normal to the dispersion relation curve at that point where the wave-normal vector meets the dispersion-relation curve.

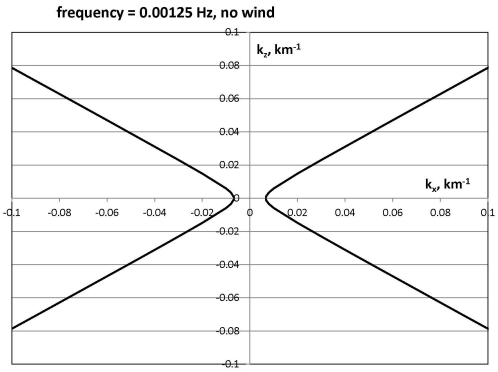

FIG. 8. Dispersion relation diagram without wind, $f = 0.00125$ Hz, $C = 0.3$ km/s, $N = 0.01$ s^{-1}, and $k_A = 0.0267$ km^{-1}. The slope of the asymptotes is determined by the ratio of N to ω. The intersection of the dispersion-relation curve with the horizontal axis is determined by k_A.

If the angle of the wave-normal direction with the horizontal axis is too large, there will be no intersection with the dispersion-relation curve, indicating that propagation is impossible in that direction (that is, the wave is evanescent in that direction). Rays whose wave-normal direction is asymptotic to the dispersion-relation diagram in figure 8 are called asymptotic waves. For asymptotic waves, once the frequency is chosen, there is only one wave-normal direction possible and only one ray direction possible. However, as can be seen from figure 8, for non-asymptotic waves there are other wave-normal directions possible, including exactly horizontal propagation.

b. Including wind

Including wind in the dispersion relation for gravity waves has a profound effect. To see that, we look at the dispersion-relation diagram with wind shown in figure 9. Downwind is to the right. The effect of wind is to bring

[3] an extraneous solution of the quartic is one in which the magnitude of k is negative.

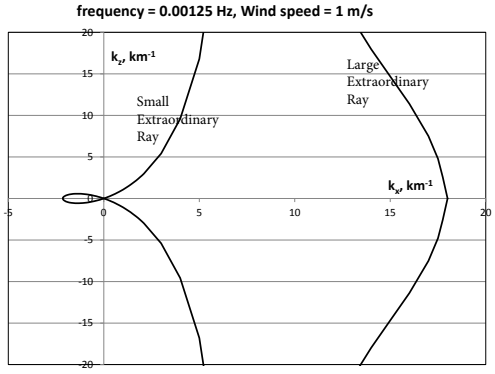

FIG. 9. Dispersion relation diagram showing the small extraordinary ray and the large extraordinary ray with 1 m/s wind blowing to the right. Otherwise, conditions as in figure 8. Figure 10 shows the detail near the origin.

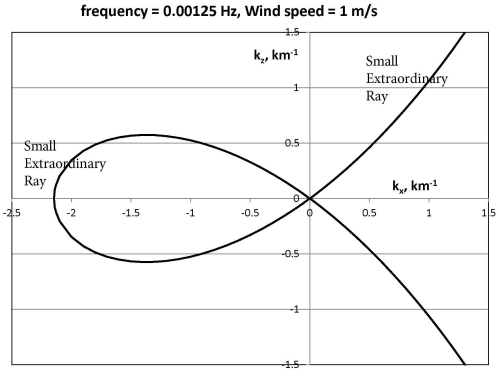

FIG. 10. Dispersion relation diagram showing the small extraordinary ray. Conditions are the same as in figure 9. Figure 11 shows the detail near the origin.

in parts of the diagram on the left and right from infinity. These parts brought in from infinity by the presence of wind, we refer to as extraordinary waves, in analogy with electromagnetic wave propagation in the ionosphere (e.g. Budden 1961; Ratcliffe 1962). The separate branch on the downwind (right) side of the diagram, we refer to as the "large extraordinary wave." The other parts of the curve (except the part near the origin), we refer to as the "small extraordinary wave." The curves continue to infinity at the top and bottom of the figure.

An expansion of figure 9 near the origin is shown in figure 10. An expansion of figure 10 near the origin is

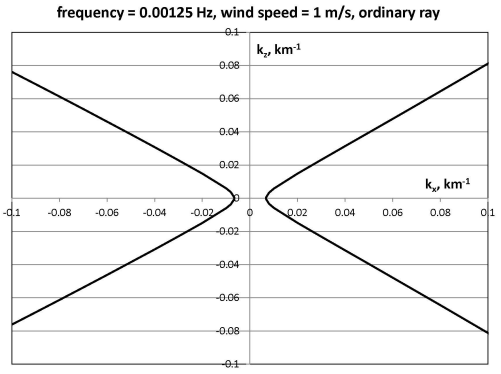

FIG. 11. Dispersion relation diagram for the ordinary ray. Conditions are the same as in figure 9. Although this dispersion relation diagram is similar to the no-wind dispersion relation diagram in Figure 8, it differs greatly far outside the plotting area.

shown in figure 11, which shows the dispersion relation diagram for the ordinary ray with wind. It is similar to the dispersion relation diagram without wind, but shifted slightly to the right.

For downwind propagation (propagation to the right in figure 10) of the small extraordinary wave at an angle θ from the horizontal, the magnitude of k in figure 10 is given approximately by taking the lower sign in (11). For upwind propagation (propagation to the left in figure 10) of the small extraordinary wave, the magnitude of k in figure 10 is given approximately by taking the upper sign in (12). For downwind propagation (propagation to the right in figure 9), the magnitude of k for the large extraordinary ray in figure 9 is given approximately by taking the upper sign in (11).

As can be seen from figures 9, 10, and 11, a straight line from the origin has the possibility of intersecting the dispersion-relation curve in four places. Thus, choosing the frequency and direction of propagation is not sufficient to determine the wave. It may be necessary to choose the type of wave desired.

For example, choosing a wave-normal direction that is nearly horizontal will give four intersections with the dispersion-relation curve. Two downwind (to the right), and two upwind (to the left). These four intersections correspond to the solutions of the quartic equation (4). The intersections near the origin give waves that are similar to the no-wind case (one upwind and one downwind), which we refer to as "ordinary waves," in analogy with electromagnetic wave propagation. The other intersection in the downwind direction, we refer to as the "large extraordinary wave," and the other intersection in the upwind direction, we refer to as the "small extraordinary wave."

As we make the wave-normal direction more vertical, we eventually reach a situation in the upwind direction in which the wave-normal vector is tangent to the dispersion-relation curve. At that point, the upwind ordinary and extraordinary waves have the same wavenumber, and we have possibility of coupling between the two types of waves. Making the wave-normal direction even more vertical will give no intersection with the dispersion-relation curve in the upwind direction, so that all such waves launched in the upwind direction will be evanescent. In that case, the quartic equation (4) will have only two real roots plus a complex pair.

The above considerations are summarized in Table 1.

The slope of the asymptotes in figures 8, 10, and 11 is $\sqrt{N^2/\omega^2 - 1}$. If θ is the angle of the wave-normal direction to the horizontal, then we have $\cos\theta = \omega/N$. When there is no wind, Figure 8 shows that gravity waves will propagate if the wave normal direction is such that the angle relative to horizontal is less than $\cos^{-1}(\omega/N)$. For ordinary waves, figure 11 shows that the same is approximately true for ordinary waves. Figure 10 shows that for upwind propagation, propagation of the small extraordinary wave is also possible if the angle of the wave normal with the horizontal is less than $\cos^{-1}(\omega/N)$. For downwind propagation, figure 10 shows that propagation of the small extraordinary wave is possible if the angle of the wave normal with the horizontal is larger than $\cos^{-1}(\omega/N)$. Figure 9 shows that propagation of the large extraordinary wave is possible only for downwind propagation, and exactly vertical propagation (wave-normal direction) of the large extraordinary wave (or any gravity wave) is not possible. However, exactly vertical propagation of the ray direction for the small extraordinary wave is possible as can be seen in figure 10.

7. Ray paths with wind

Including wind alters the gravity-wave ray paths. We demonstrate this using a wind model in which a wind blowing toward the East starts at zero on the ground and increases linearly to 5 m/s at 500 km. As with the no-wind case in figure 7, the source is at a height of 5 km, and the elevation angle of transmission is stepped from 10° to 90° in steps of 5°. Although such a simple wind model is not a realistic wind profile, it is useful here to illustrate the effect of wind on ray paths.

The ray paths for transmission downwind and upwind of the "ordinary ray" are shown in figures 12 and 13, respectively. Although these ray paths are similar to the no-wind case in figure 7, the waves are blown downwind, and the reflection heights differ from the no-wind case in figure 7.

Figures 14 and 15 show downwind and upwind ray paths respectively for the "small extraordinary ray." As can be seen, these rays differ greatly from those of the no-wind case in figure 7.

Ray paths for the "large extraordinary ray" are not shown because they were not interesting as they stayed within a few kilometers of the ground. For the large extraordinary rays, only rays launched downwind are not evanescent at the source. As can be seen from figure 9,

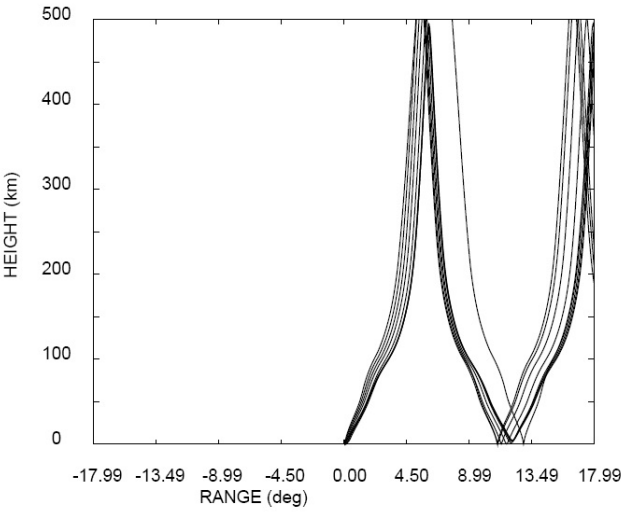

FIG. 12. Ordinary ray, downwind, f= 0.00125 Hz (wind starts at zero on the ground and increases linearly to 5 m/s at 500 km). Otherwise, conditions as in figure 7. The 10° elevation-angle ray reaches an apogee of 486 km at a range of 689 km in 3 hours. The 50° elevation-angle ray reaches an apogee of 709 km at a range of 724 km in 10 hours.

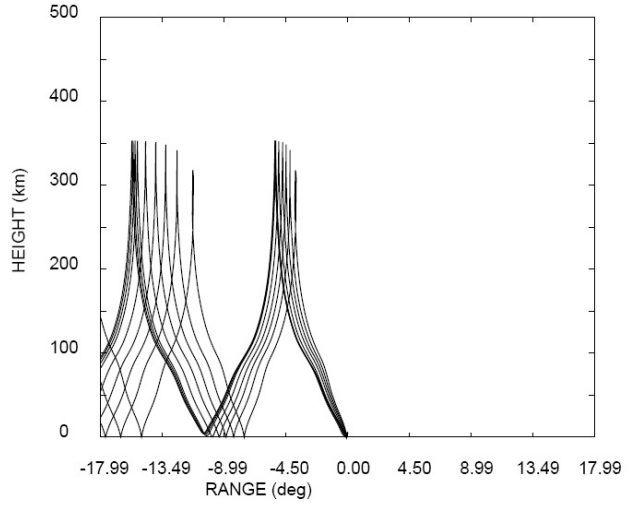

FIG. 13. Ordinary ray, upwind, f= 0.00125 Hz. Otherwise, conditions as in figure 12. The 10° elevation-angle ray reaches an apogee of 353 km at a range of 589 km in 2 hours. The 50° elevation-angle ray reaches an apogee of 318 km at a range of 422 km in 3.6 hours.

TABLE 1. Categories of the roots of the quartic equation that determines the magnitude of the wavenumber. The four roots are assumed to be ordered from left to right in increasing value of the real part of the root. Thus, Root 1 is the largest negative root, while Root 4 is the largest positive root. n_{sol} is the number of real roots. It is clear from figures 9, 10, and 11 that the number of real roots is 2 or 4 and that two roots of the quartic have negative real parts and two roots have positive real parts. When there are only two real roots, propagation in the upwind direction is evanescent, and propagation in the downwind direction is possible only for the two types of extraordinary wave. $\mathbf{k}\cdot\mathbf{v}$ is positive for downwind propagation, negative for upwind propagation. Extraneous roots are roots with negative wavenumber.

		Extraneous Roots (Real part < 0)				Wanted Roots (Real part > 0)			
		Root 1		Root 2		Root 3		Root 4	
n_{sol}	$k\cdot v$	Propagating	Evanescent	Propagating	Evanescent	Propagating	Evanescent	Propagating	Evanescent
4	< 0	Large Extraordinary		Ordinary		Ordinary		Small Extraordinary	
2	< 0	Large Extraordinary		Small Extraordinary			Ordinary		Small Extraordinary
4	> 0	Small Extraordinary		Ordinary		Ordinary		Large Extraordinary	
2	> 0		Small Extraordinary		Ordinary	Small Extraordinary		Large Extraordinary	

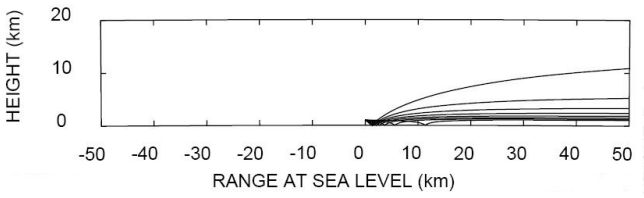

FIG. 14. Small extraordinary ray, downwind, f= 0.00125 Hz. Elevation angle of transmission varies from 50° through 85° in steps of 5°. Rays for elevation angles of transmission of 10° through 45° and 90° were evanescent at the source. The 50° elevation angle of transmission had rays that got the highest and had a pulse travel time of 88 hours. The 55° elevation angle of transmission had a pulse travel time of 233 hours. The source height is 1 km. Otherwise, conditions as in figure 12.

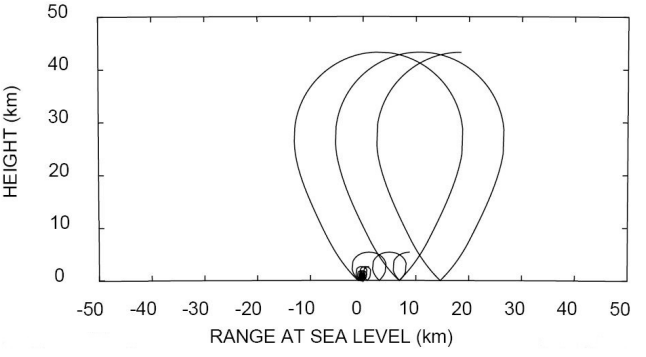

FIG. 15. Small extraordinary ray, upwind, f= 0.00125 Hz. Elevation angle of transmission varies from 10° through 45° in steps of 5°. Rays for elevation angles of 50° through 90° were evanescent at the source. Rays for 45° elevation angles reached the highest and had a pulse travel time of 62 hours to the apogee and a total of 122 hours from the source back down to the first ground reflection. Rays for 40° elevation angles reached a height of 5.4 km with a pulse travel time of 50 hours and a total of 93 hours from the source back down to the first ground reflection. Otherwise, conditions as in figure 14.

large extraordinary rays exist only in the downwind direction.

Although large extraordinary waves seem to be of no importance for long-range propagation, it is important to know of their existence. In addition, extraordinary waves may be important for dissipation of gravity-wave energy.

8. Comparison with other calculations

Comparison with other work is useful to add confidence to the present analysis and to give further insight into the propagation of gravity waves.

Figures 16 and 17 (Georges 1971, Figure 4, page 40) show examples of downwind and upwind propagation, respectively. All of these examples are for a wavelength of 10 km, and various frequencies and elevation angles of transmission. It is clear from comparing figures 16 and 17 with figures 12, 13, 14, and 15, that the rays in figures 16 and 17 are for "small extraordinary rays," not "ordinary rays."

Because wavelength at the source was specified in figures 16 and 17, rather than frequency, each ray path in those two figures for the various elevation angles of transmission has a different frequency. Because those frequencies were not given in the publication (Georges 1971), we had to experiment by varying frequency until we got a wavelength of 10 km in each of our comparisons. To simplify the comparisons, we decided to make ray path calculations for only the 60° elevation angle of transmission.

Although the source was on the ground in the ray path calculations in figures 16 and 17, we chose to move the source slightly off the ground to a height of 0.5 km for our comparisons because the wind speed is zero on the ground for this model, and the "small extraordinary" rays

would not exist there when specifying frequency rather than specifying wavenumber.

Figures 18 and 19 show the comparison ray paths we calculated for an elevation angle of transmission of plus and minus 60°, for both downwind and upwind propagation.

Figure 18 is for transmitting a small extraordinary ray downwind. The roots of the quartic equation at the source are $Ck = 250$ sec^{-1} (large extraordinary wave), 0.19 sec^{-1} (small extraordinary wave), and -0.36 $\pm$ 0.79 i sec^{-1} (evanescent ordinary and small extraordinary waves), where C is the local speed of sound. The calculation is for the small extraordinary wave, and the frequency was adjusted to give a wavelength of about 10 km.

The ray in the upwind case in figure 19 starts as an "ordinary ray," but couples to a "small extraordinary ray" at a height of about 3.5 km. The roots of the quartic equation at the source are $Ck = 0.88$ sec^{-1} (small extraordinary wave), 0.19 sec^{-1} (ordinary wave), -0.015 sec^{-1} (extraneous[4] ordinary wave), and -250 sec^{-1} (extraneous large extraordinary wave). The calculation is for transmitting an ordinary wave. However, something interesting happens to the ray at a height of 3.6975 km. At that height, the roots of the quartic are $Ck = 0.19$ sec^{-1} (small extraordinary wave), 0.19 sec^{-1} (ordinary wave), -0.095 sec^{-1} (extraneous ordinary wave), and -33 sec^{-1} (extraneous large extraordinary wave). At that height, the wavenumbers for the ordinary wave and the small extraordinary wave are equal, and the ray tracing program has started to calculate the ray for the small extraordinary wave from this height upward. At a height of 10 km, the roots of the quartic are $Ck = 0.19$ sec^{-1} (small extraordinary wave), 0.10 sec^{-1} (ordinary wave), -0.065 sec^{-1} (extraneous ordinary wave), and -12 sec^{-1} (extraneous large extraordinary wave), and the ray tracing program is integrating a ray for which $Ck = 0.19$ sec^{-1}. The ray tracing program uses the quartic only when beginning a ray path calculation for initializing the wavenumber. After that, it uses the roots of the quartic only for comparison to identify what ray is being calculated. So, the ray path shown in figure 19 is a small extraordinary wave, and this is an example of wave coupling. However, ray identification is difficult when two kinds of rays have nearly equal wavelengths.

The downwind case (figure 18) agrees reasonably well with figure 16, but the upwind case (figure 19) agrees only qualitatively with figure 17. The disagreement might be because the source in figures 16 and 17 was on the ground (where there was no wind), whereas we put the source at a height of 0.5 km, where it was possible to have an extraordinary wave because there is wind at that height.

Here is the explanation of the upwind ray paths for the small extraordinary wave in figure 19 in terms of the dispersion-relation diagram in figure 10. The source

[4] An extraneous wave corresponds to a negative value for the magnitude of the wavenumber.

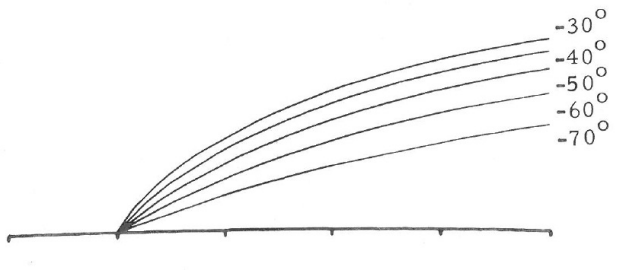

FIG. 16. Ray paths for internal gravity waves, all with a total wavelength of 10 km, as the initial direction of phase propagation (labeled on the curves) is varied. The atmosphere is isothermal and wind increases linearly with height by 0.1 m/s/km, blowing to the right. Scale is 100 km/div. The vertical scale is the same as the horizontal scale. (Georges 1971, Figure 4, page 40)

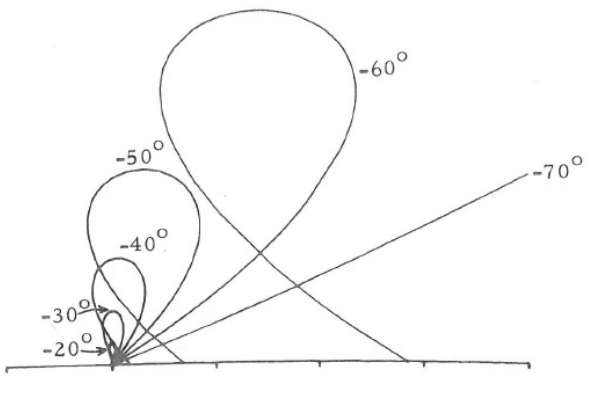

FIG. 17. Ray paths for internal gravity waves, all with a total wavelength of 10 km, as the initial direction of phase propagation (labeled on the curves) is varied. The atmosphere is isothermal and wind increases linearly with height by 0.1 m/s/km, blowing to the left. Otherwise, conditions as in figure 16. Scale is 100 km/div. The vertical scale is the same as the horizontal scale.

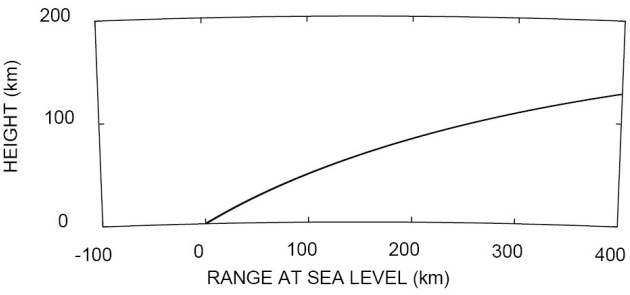

FIG. 18. Ray paths for internal gravity waves, small extraordinary ray, downwind. f = 0.00163946 Hz, $\lambda = 10.0021$ km at the source, elevation angle of transmission is $\pm 60°$, source height is 0.5 km. The atmosphere is isothermal and wind increases linearly with height by 0.1 m/s/km. Otherwise, conditions as in figure 16. The pulse travel time is about 4.7 hours.

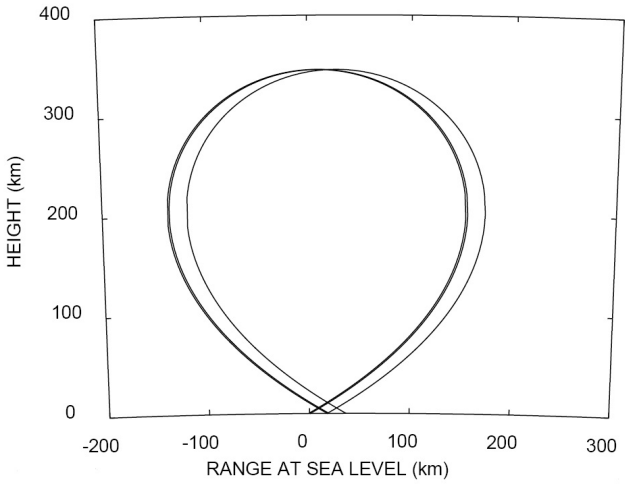

FIG. 19. Ray paths for internal gravity waves, upwind. f = 0.00163446 Hz, $\lambda = 9.8$ km at the source. Wind is blowing to the left. The atmosphere is isothermal and wind increases linearly with height by 0.1 m/s/km. Otherwise, conditions as in figure 18. The pulse travel time is about 6 hours from the source to the apogee. The total pulse travel time from the source back down to the first ground reflection is about 10 hours.

height is 0.5 km. The ray begins as an ordinary ray, but very quickly couples to a small extraordinary ray. Near the ground, the wind speed is very small, so the dispersion relation for the small extraordinary wave in figure 10 is expanded out to the left very far. in that case, there is very little difference between the small extraordinary wave and the ordinary wave. We start with the wave-normal direction to be - 60 degrees in the upwind direction. This give a ray direction that is up and also in the upwind direction. As the ray moves up, the wind speed increases, and the loop in figure 10 for the upwind dispersion-relation diagram in figure 10 gets smaller. As the small extraordinary wave propagates, the horizontal component of the wave vector k stays constant because the medium varies only in the vertical direction. To keep the horizontal component of k constant while the dispersion-relation diagram gets smaller, the wave-normal direction must change to be more horizontal. Since the wave normal is pointing downward, it will be pointing less downward. At a certain point, the wave-normal direction will intersect the dispersion-relation diagram at a point where the dispersion relation diagram is horizontal. At that point, the ray direction will be pointing exactly up. As the ray continues upward, the dispersion-relation diagram continues to contract as the wind speed increases, and the wave-normal direction continues to be more horizontal to keep the horizontal component of k constant. At that point, the ray direction is still upward, but the horizontal component of the ray direction is now downwind even though the horizontal component of the wave-normal direction is still upwind. As the ray continues upward, the wind speed continues to increase, and the dispersion relation diagram continues to contract. Eventually, the wave-normal direction becomes horizontal (still in the upwind direction), and the ray direction also becomes horizontal, but in the downwind direction. At that point, the ray is at the apogee, and will begin to come back down. As the ray starts down, the wind speed decreases, the dispersion-relation diagram expands, and the wave-normal direction moves upward to keep the horizontal component of k constant. As the ray continues downward, the wind speed continues to decrease, the dispersion relation diagram continues to expand, and the angle of the wave normal with the horizontal continues to increase, we eventually reach a point where the k vector intersects the dispersion-relation diagram at a point where the dispersion relation diagram is horizontal. At that point, the ray direction is exactly down. As the ray continues downward, the wind speed continues to decrease, the dispersion-relation diagram continues to expand, and the angle of the wave normal with the horizontal continues to increase, the ray direction will again be pointing upwind and downward. Eventually, the ray gets back to the starting height, then continues downward, where it reflects from the ground, and repeats the cycle. This explains the loops in figure 19. The same explanation applies to the ray paths in figure 15 as well, except that the ray paths in figure 15 are small extraordinary rays throughout, with no coupling from an ordinary ray.

The behavior of the rays for downwind propagation of the small extraordinary ray in figures 14 and 18 can be explained similarly in terms of contracting and expanding of the dispersion-relation diagram as the ray moves up or down and the wind speed increases or decreases.

9. Examples of possible meteorological application areas of a gravity wave ray trace program

The downdrafts from severe weather produce density currents. These density currents can in turn produce a variety of wave disturbances. Researchers have documented with case studies numbers of situations where atmospheric gravity waves occurred in conjunction with or resulting from density currents. Examples of case studies include the work of Knupp (2006) who performed an observational analysis of a gust front to bora to solitary wave transition within an evolving nocturnal boundary layer. Doviak and Ge (1984) studied an atmospheric solitary wave observed with a Doppler radar, a tall tower, and a surface network. Zhang and Fritsch (1988) documented relationships between Internal gravity waves and a squall line. Fulton et al. (1990) analyzed the Initiation of a solitary wave family in the demise of a nocturnal thunderstorm density current, also showing an example of the waves embedded within the current. Haase and Smith (1984): detail a case study of morning glory wave clouds in Oklahoma.

These observations typically involved extensive observational systems (e.g surface networks, soundings, Doppler radars, Doppler lidars, towers or aircraft). Historically, only very limited numbers of cases were observed in sufficient detail to enable modelling.

We suggest that one valuable application of a gravity wave ray trace program would be to perform sensitivity studies, for example, varying the height and strength of ground based inversions relative to atmospheric gravity wave propagation characteristics. It will be interesting to determine situations where rays leak out of waveguides to the upper atmosphere resulting in gravity wave dissipation.

Atmospheric gravity waves can have important roles in initiating convection, as well as being initiated by convection. Such meteorological processes could be used to examine possible roles of ordinary and extraordinary gravity waves. If a physical process generates gravity waves, the type of wave created can determine whether or not the possibility of new convection is likely. For example, a downdraft impacting a quiescent environment can only create an ordinary gravity wave. If there is a ground based regional inversion present, energy can be transferred horizontally with minimal loss to the upper atmosphere.

If in contrast, downdrafts descend into existing outflows from previous storms other types of gravity wave initiation are possible. It will be valuable to explore a variety of such situations.

10. Concluding remarks

We have shown that although acoustic-gravity-wave ray tracing has been widely applied, there are some interesting features that add a certain complexity, interest, and difficulty. Choosing the frequency and launch angle (of the wave-normal direction) in the presence of wind gives a quartic equation to determine the wavenumber. This means that in addition to specifying the usual parameters of source location, frequency, and transmission direction, it is necessary to specify what kind of ray one wants (ordinary, small extraordinary, or large extraordinary). Notice that this is analogous to specifying ordinary or extraordinary waves for radio waves in the ionosphere (e.g. Budden 1961; Ratcliffe 1962) or characteristic polarization for light waves in birefringent crystals.

The distinction between ordinary and extraordinary gravity waves has apparently not previously been noticed, in spite of the fact that all of the example ray paths presented by Georges (1971) were extraordinary rays.

Although "geometrical phase" (also called "Berry phase" or "additional memory") (Berry 1990; Budden and Smith 1976; Smith 1975; Weinberg 1962) can have a noticeable effect on the WKB approximation, including "geometrical phase" does not change the dispersion relation or the ray paths (Weinberg 1962, Section IV).[5]

In the future, we plan to apply the CIRES/NOAA atmospheric gravity wave ray tracing program to meteorological cases where detailed observations are available, such as those in Antarctica (e.g. Chen et al. 2013, 2016; Zhao et al. 2017), or interesting processes have been identified (e.g. leakage of gravity wave energy from ducts formed by ground-based stable layers).

Acknowledgments. The authors thank William Otto and Wendi Madsen for their assistance in upgrading the ray tracing program to be compatible with present-day compilers and loaders. We thank Emily Gu for help in making many of the calculations presented here. We also acknowledge Xinzhao Chu for discussions on the paper presentation. This research was partially supported by the National Science Foundation (NSF) grants PLR-1246405 and AGS-1136272.

References

Alexander, M. J., 1996: A simulated spectrum of convectively generated gravity waves: Propagation from the tropopause to the mesopause and effects on the middle atmosphere. *Journal of Geophysical Research: Atmospheres*, **101 (D1)**, 1571–1588, doi:10.1029/95JD02046, URL http://dx.doi.org/10.1029/95JD02046.

Arai, N., M. Iwakuni, S. Watada, Y. Imanishi, T. Murayama, and M. Mogami, 2011: Atmospheric boundary waves excited by the tsunami generation related to the 2011 great tohoku-oki earthquake. *Geophys. Res. Lett.*, **38**, L00G18, doi:10.1029/2011GL049146, L00G18, doi:10.1029/2011GL049146.

Artru, J., V. Ducic, H. Kanamori, and P. Lognonné, 2005: Ionospheric detection of gravity waves induced by tsunamis. *Geophys. J. Int.*, **160**, 840–848, doi:10.1111/j.1365-246X.2005.0255.x, doi:10.1111/j.1365-246X.2005.0255.x.

Balachandran, N. K., 1980: Gravity waves from thunderstorms. *Monthly Weather Review*, **108 (6)**, 804–816, doi:10.1175/1520-0493(1980)108⟨0804:GWFT⟩2.0.CO;2, URL https://doi.org/10.1175/1520-0493(1980)108⟨0804:GWFT⟩2.0.CO;2.

Bedard, A. J., Jr., 1982: Sources and detection of atmospheric wind shear. *AIAA Journal*, **20**, 940–945.

Bedard, A. J., Jr., 1984: Optimizing the use of surface sensors for wind shear detection. *J. Aircraft*, **21**, 971–977.

Bedard, A. J., Jr., F. Canavero, and F. Einaudi, 1986: Atmospheric gravity waves and aircraft turbulence encounters. *Journal of the Atmospheric Sciences*, **43 (23)**, 2838–2844, doi:10.1175/1520-0469(1986)043⟨2838:AGWAAT⟩2.0.CO;2, URL https://doi.org/10.1175/1520-0469(1986)043⟨2838:AGWAAT⟩2.0.CO;2.

Bedard, A. J., Jr., and R. M. Jones, 2013: Infrasonic ray tracing applied to mesoscale atmospheric structures: Refraction by hurricanes. *J. Acoust. Soc. Am.*, **134 (5)**, 3446–3451, doi:10.1121/1.4823802.

Bedard, A. J., Jr, R. Nagle, and T. LeFebvre, 1981: Monostatic acoustic sounder measurements during project AEOLUS 1980: Case studies

[5]Notice that (Weinberg 1962, eq. 136) is the three-dimensional analog of (Budden and Smith 1976, eq. 6).

describing the erosion of surface-based stable layers. *Proceedings, International Symposium on Acoustic Remote Sensing of the Atmosphere and Oceans*, june 22-25, 1981, The University of Calgary, Calgary, Alberta, Canada, VI-27VI57. Published August 1982.

Bedard, A. J., Jr., and Coauthors, 2004: Overview of the ISNet data set and conclusions and recommendations from a march 2003 workshop to review ISNet data. *Proceedings 22nd Conference on Severe Local Storms*, 4-8 October 2004, Hyanis, MA, Sponsored by the Amer. Meteorol. Soc., Boston, MA.

Beluši'c, D., M. Pasarić, and M. Orlić, 2004: Quasi-periodic bora gusts related to the structure of the troposphere. *Quarterly Journal of the Royal Meteorological Society*, **130 (598)**, 1103–1121, doi:10.1256/qj.03.53, URL http://dx.doi.org/10.1256/qj.03.53.

Berry, M. V., 1990: Budden & Smith's 'additional memory' and the geometrical phase. *Proc. R. Soc. London, Ser. A*, **431**, 531–537.

Booker, J. R., and F. P. Bretherton, 1967: The critical layer for internal gravity waves in a shear flow. *Journal of Fluid Mechanics*, **27 (03)**, 513–539.

Bowman, H. S., and A. J. Bedard, 1971: Observations of infrasound and subsonic disturbances related to severe weather. *Geophysical Journal of the Royal Astronomical Society*, **26 (1-4)**, 215–242, doi:10.1111/j.1365-246X.1971.tb03396.x, URL http://dx.doi.org/10.1111/j.1365-246X.1971.tb03396.x.

Brillouin, L., 1926: La mécanique ondulatoire de Schrödinger; une méthode générale de résolution par approximations successives. *Academie des sciences, Paris*, **183**, 24–26.

Broutman, D., J. W. Rottman, , and S. D. Eckermann, 2004: Ray methods for internal waves in the atmosphere and ocean. *Annual Review of Fluid Mechanics*, **36 (1)**, 233–253, doi:10.1146/annurev.fluid.36.050802.122022, URL https://doi.org/10.1146/annurev.fluid.36.050802.122022.

Budden, K. G., 1961: *Radio waves in the ionosphere*. University Press, Cambridge, 542 pp.

Budden, K. G., and M. S. Smith, 1976: Phase memory and additional memory in WKB solutions for wave propagation in stratified media. *Proc. R. Soc. London, Ser. A*, **350**, 27–46.

Chen, C., X. Chu, A. J. McDonald, S. L. Vadas, Z. Yu, W. Fong, and X. Lu, 2013: Inertia-gravity waves in antarctica: A case study using simultaneous lidar and radar measurements at McMurdo/Scott Base (77.8°S, 166.7°E). *Journal of Geophysical Research: Atmospheres*, **118 (7)**, 2794–2808, doi:10.1002/jgrd.50318, URL http://dx.doi.org/10.1002/jgrd.50318.

Chen, C., X. Chu, J. Zhao, B. R. Roberts, Z. Yu, W. Fong, X. Lu, and J. A. Smith, 2016: Lidar observations of persistent gravity waves with periods of 3-10 h in the Antarctic middle and upper atmosphere at McMurdo (77.83°S, 166.67°E). *Journal of Geophysical Research: Space Physics*, **121 (2)**, 1483–1502, doi:10.1002/2015JA022127, URL http://dx.doi.org/10.1002/2015JA022127, 2015JA022127.

Chimonas, G., and C. O. Hines, 1970: Atmospheric gravity waves induced by a solar eclipse. *Journal of Geophysical Research*, **75 (4)**, 875–875, doi:10.1029/JA075i004p00875, URL http://dx.doi.org/10.1029/JA075i004p00875.

Chmyrev, V., V. Marchenko, O. Pokhotelov, L. Stenflo, A. Streltsov, and Å. Steen, 1991: Vortex structures in the ionosphere and the magnetosphere of the earth. *Planetary and Space Science*, **39 (7)**, 1025 – IN4, doi:http://dx.doi.org/10.1016/0032-0633(91)90108-M, URL http://www.sciencedirect.com/science/article/pii/003206339190108M.

Christie, D. R., and P. Campus, 2009: *The IMS Infrasound Network: Design and Establishment of Infrasound Stations*, 29–75. Springer Netherlands, Dordrecht, doi:10.1007/978-1-4020-9508-5_2, URL http://dx.doi.org/10.1007/978-1-4020-9508-5_2.

Chu, X., Z. Yu, C. S. Gardner, C. Chen, and W. Fong, 2011: Lidar observations of neutral Fe layers and fast gravity waves in the thermosphere (110-155 km) at McMurdo (77.8°S, 166.7°E), antarctica. *Geophysical Research Letters*, **38 (23)**, doi:10.1029/2011GL050016, URL http://dx.doi.org/10.1029/2011GL050016, L23807.

Cowling, D. H., H. D. Webb, and K. C. Yeh, 1971: Group rays of internal gravity waves in a wind-stratified atmosphere. *Journal of Geophysical Research*, **76 (1)**, 213–220, doi:10.1029/JA076i001p00213, URL http://dx.doi.org/10.1029/JA076i001p00213.

Cunningham, W. J., and A. J. Bedard, 1993: Mountain valley evacuation by upper level flows - a scale model study. *AIAA Journal*, **31 (9)**, 1569–1573, doi:10.2514/3.11816, URL https://doi.org/10.2514/3.11816, publisher: American Institute of Aeronautics and Astronautics.

Curry, M. J., and R. C. Murty, 1974: Thunderstorm-generated gravity waves. *Journal of the Atmospheric Sciences*, **31 (5)**, 1402–1408, doi:10.1175/1520-0469(1974)031⟨1402:TGGW⟩2.0.CO;2, URL https://doi.org/10.1175/1520-0469(1974)031⟨1402:TGGW⟩2.0.CO;2.

Deardorff, J. W., G. E. Willis, and D. K. Lilly, 1969: Laboratory investigation of non-steady penetrative convection. *Journal of Fluid Mechanics*, **35**, 7–31, doi:10.1017/S0022112069000942.

Ding, F., W. Wan, and H. Yuan, 2003: The influence of background winds and attenuation on the propagation of atmospheric gravity waves. *Journal of Atmospheric and Solar-Terrestrial Physics*, **65 (7)**, 857–869, doi:http://dx.doi.org/10.1016/S1364-6826(03)00090-7, URL http://www.sciencedirect.com/science/article/pii/S1364682603000907.

Doviak, R. J., and R. Ge, 1984: An atmospheric solitary gust observed with a Doppler radar, a tall tower and a surface network. *Journal of the Atmospheric Sciences*, **41 (17)**, 2559–2573, doi:10.1175/1520-0469(1984)041⟨2559:AASGOW⟩2.0.CO;2, URL https://doi.org/10.1175/1520-0469(1984)041⟨2559:AASGOW⟩2.0.CO;2.

Eckart, C., 1960: *Hydrodynamics of Oceans and Atmospheres*. Pergamon Press, Oxford, 290 pp.

Einaudi, F., A. J. Bedard, Jr., and J. J. Finnigan, 1989: A climatology of gravity waves and other coherent disturbances at the boulder atmospheric observatory during marchapril 1984. *Journal of the Atmospheric Sciences*, **46 (3)**, 303–329, doi:10.1175/1520-0469(1989)046⟨0303:ACOGWA⟩2.0.CO;2, URL https://doi.org/10.1175/1520-0469(1989)046⟨0303:ACOGWA⟩2.0.CO;2.

Einaudi, F., and C. O. Hines, 1970: WKB approximation in application to acoustic-gravity waves. *Can. J. Phys.*, **48**, 1458–1471.

Fritts, D. C., and M. J. Alexander, 2003: Gravity wave dynamics and effects in the middle atmosphere. *Rev. Geophys.*, **41 (1)**, doi:10.1029/2001RG000106, URL http://dx.doi.org/10.1029/2001RG000106, paper number 1003.

Fritts, D. C., and M. J. Alexander, 2012: Correction to "gravity wave dynamics and effects in the middle atmosphere". *Rev. Geophys.*, **50 (3)**, doi:10.1029/2012RG000409, URL http://dx.doi.org/10.1029/2012RG000409, paper number RG3004.

Fritts, D. C., and Coauthors, 2016: The deep propagating gravity wave experiment (DEEPWAVE): An airborne and ground-based exploration of gravity wave propagation and effects from their sources throughout the lower and middle atmosphere. *Bulletin of the American Meteorological Society*, **97 (3)**, 425–453, doi:10.1175/BAMS-D-14-00269.1, URL https://doi.org/10.1175/BAMS-D-14-00269.1.

Fulton, R., D. S. Zrnić, and R. J. Doviak, 1990: Initiation of a solitary wave family in the demise of a nocturnal thunderstorm density current. *Journal of the Atmospheric Sciences*, **47 (3)**, 319–337, doi:10.1175/1520-0469(1990)047⟨0319:IOASWF⟩2.0.CO;2, URL https://doi.org/10.1175/1520-0469(1990)047⟨0319:IOASWF⟩2.0.CO;2.

Georges, T. M., 1971: A program for calculating three-dimensional acoustic-gravity ray paths in the atmosphere. Technical Report ERL 212-WPL 16, Natl. Oceanic and Atmos. Admin. 43 pp.

Georges, T. M., R. M. Jones, and R. S. Lawrence, 1990: A PC version of the HARPO ocean acoustic ray-tracing program. Tech. Memo ERL WPL-180, Natl. Oceanic and Atmos. Admin., Boulder, Colorado. 18 pp. (program available at http://cires.colorado.edu/∼mjones/raytracing/programs.htm).

Gerrard, A. J., Y. Bhattacharya, and J. P. Thayer, 2011: Observations of in-situ generated gravity waves during a stratospheric temperature enhancement (ste) event. *Atmospheric Chemistry and Physics*, **11 (22)**, 11 913–11 917, doi:10.5194/acp-11-11913-2011, URL https://www.atmos-chem-phys.net/11/11913/2011/.

Gossard, E. E., and W. H. Hooke, 1975: *Waves in the Atmosphere*. Elsevier Scientific Publishing Company, Amsterdam, 456 pp.

Haase, S. P., and R. K. Smith, 1984: Morning glory wave clouds in oklahoma: A case study. *Monthly Weather Review*, **112 (10)**, 2078–2089, doi:10.1175/1520-0493(1984)112⟨2078:MGWCIO⟩2.0.CO;2, URL https://doi.org/10.1175/1520-0493(1984)112⟨2078:MGWCIO⟩2.0.CO;2.

Hickey, M., and K. Cole, 1987: A quartic dispersion equation for internal gravity waves in the thermosphere. *Journal of Atmospheric and Terrestrial Physics*, **49 (9)**, 889 – 899, doi:http://dx.doi.org/10.1016/0021-9169(87)90003-1, http://dx.doi.org/10.1016/0021-9169(87)90003-1.

Hickey, M. P., G. Schubert, and R. L. Walterscheid, 2009: Propagation of tsunami-driven gravity waves into the thermosphere and ionosphere. *J. Geophys. Res.*, **114**, A08304, doi:10.1029/2009JA014105, A08304, doi:10.1029/2009JA014105.

Hung, R., and J. Kuo, 1978: Ionospheric observation of gravity-waves associated with hurricane eloise. *Journal of Geophysics-Zeitschrift Für Geophysik*, **45 (1)**, 67–80.

Hung, R. J., T. Phan, and R. E. Smith, 1979: Coupling of ionosphere and troposphere during the occurrence of isolated tornadoes on november 20, 1973. *Journal of Geophysical Research: Space Physics*, **84 (A4)**, 1261–1268, doi:10.1029/JA084iA04p01261, URL http://dx.doi.org/10.1029/JA084iA04p01261.

Hung, R. J., and R. E. Smith, 1978: Ray tracing of gravity waves as a possible warning system for tornadic storms and hurricanes. *Journal of Applied Meteorology*, **17 (1)**, 3–11, doi:10.1175/1520-0450(1978)017⟨0003:RTOGWA⟩2.0.CO;2, URL https://doi.org/10.1175/1520-0450(1978)017⟨0003:RTOGWA⟩2.0.CO;2.

Jeffreys, H., 1923: On certain approximate solutions of linear differential equations of the second order. *Proc. London, Math. Soc. Ser. 2*, **23**, 428–436.

Jones, R. M., 1996: Three dimensional ray tracing in the atmosphere. *THE UPPER ATMOSPHERE*, W. Dieminger, G. Hartmann, and R. Leitinger, Eds., Springer Verlag, Berlin-Heidelberg, chap. II.3.1.4, 307–327, errata available at (Jones 2007, http://cires.colorado.edu/∼mjones/pubs/errata2.htm, date last viewed 26 February 2015).

Jones, R. M., 2001: The dispersion relation for internal acoustic-gravity waves in a baroclinic fluid. *Physics of Fluids*, **13**, 1274–1280, doi:http://dx.doi.org/10.1063/1.1359419, errata available at (Jones 2012, http://cires.colorado.edu/∼mjones/pubs/errata9.pdf, date last viewed 13 May 2016).

Jones, R. M., 2005: A general dispersion relation for internal gravity waves in the atmosphere or ocean, including baroclinicity, vorticity, and rate of strain. *J. Geophys. Res.*, **110, D22106**, doi:10.1029/2004JD005654, doi: 10.1029/2004JD005654, Errata available at (Jones 2008a, http://cires.colorado.edu/∼mjones/pubs/errata7.pdf, date last viewed 13 May 2016).

Jones, R. M., 2006: Minimum and maximum propagation frequencies for internal gravity waves. *J. Geophys. Res.*, **111, D06109**, doi:10.1029/2005JD006189, doi:10.1029/2005JD006189, Errata available at (Jones 2008b, http://cires.colorado.edu/∼mjones/pubs/errata8.pdf, date last viewed 13 May 2016).

Jones, R. M., 2007: Errata: Three dimensional ray tracing in the atmosphere, pp. 307-327 in THE UPPER ATMOSPHERE, editors W. Dieminger, G. Hartmann, and R. Leitinger, springer verlag, berlin-heidelberg 1996, 1014 pages., errata available at http://cires.colorado.edu/∼mjones/pubs/errata2.htm (date last viewed 26 February 2015).

Jones, R. M., 2008a: Errata: A general dispersion relation for internal gravity waves in the atmosphere or ocean, including baroclinicity, vorticity, and rate of strain, *J. Geophys. Res.*, 2005, doi: 10.1029/2004JD005654, Errata available at http://cires.colorado.edu/∼mjones/pubs/errata7.pdf (date last viewed 13 May 2016).

Jones, R. M., 2008b: Errata: Minimum and maximum propagation frequencies for internal gravity waves, *J. Geophys. Res.*, 2006, doi: 10.1029/2005JD006189, Errata available at http://cires.colorado.edu/∼mjones/pubs/errata8.pdf (date last viewed 13 May 2016).

Jones, R. M., 2012: Errata: The dispersion relation for internal acoustic-gravity waves in a baroclinic fluid, *Physics of Fluids*, 2001, 1274-1280, Errata available at http://cires.colorado.edu/∼mjones/pubs/errata9.pdf (date last viewed 13 May 2016).

Jones, R. M., and A. J. Bedard, Jr., 2015: Infrasonic ray tracing applied to small-scale atmospheric structures: Thermal plumes and updrafts/downdrafts. *J. Acoust. Soc. Am.*, **137 (2)**, 625–632, doi:10.1121/1.4906175.

Jones, R. M., L. A. Ostrovsky, and A. J. Bedard, Jr., 2017: Ionospheric effects of magneto-acoustic-gravity waves: Dispersion relation. *J. Atmos. Sol. Terr. Phys.*, **157-158**, 90–, doi:10.1016/j.jastp.2017.04.004, URL http://dx.doi.org/10.1016/j.jastp.2017.04.004.

Jones, R. M., J. P. Riley, and T. M. Georges, 1986a: HARPA - A versatile three-dimensional Hamiltonian ray-tracing program for acoustic waves in the atmosphere above irregular terrain. NOAA Special Report, GovDoc No. C55.602:H 18; GPO Item No. 207-C-1; PB87132031, National Oceanic and Atmospheric

Administration, Boulder, Colorado, 410 pp. 410 pp., report available at http://cires.colorado.edu/∼mjones/pubs/harpa.pdf (date last viewed 25 July 2016), program available at http://cires.colorado.edu/∼mjones/raytracing (date last viewed 25 July 2016).

Jones, R. M., J. P. Riley, and T. M. Georges, 1986b: HARPO - A versatile three-dimensional Hamiltonian ray-tracing program for acoustic waves in an ocean with irregular bottom. NOAA Special Report, GovDoc No. C55.602:H 23; GPO Item No. 0207-C-01; PB87172573, National Oceanic and Atmospheric Administration, Boulder, Colorado, 455 pp. 455 pp., report available at http://cires.colorado.edu/∼mjones/pubs/harpo.pdf (date last viewed 25 July 2016), program available at http://cires.colorado.edu/∼mjones/raytracing (date last viewed 25 July 2016).

Jones, W. L., 1969: Ray tracing for internal gravity waves. *Journal of Geophysical Research*, **74 (8)**, 2028–2033, doi:10.1029/JB074i008p02028, URL http://dx.doi.org/10.1029/JB074i008p02028.

Jurén, C., and L. Stenflo, 1973: On resonant interaction of atmospheric waves. *Radio Science*, **8 (7)**, 651–652, doi:10.1029/RS008i007p00651.

Knupp, K., 2006: Observational analysis of a gust front to bore to solitary wave transition within an evolving nocturnal boundary layer. *Journal of the Atmospheric Sciences*, **63 (8)**, 2016 – 2035, URL http://search.ebscohost.com/login.aspx?direct=true&db=aph&AN=21860940&site=ehost-live&scope=site.

Kramers, H. A., 1926: Wellenmechanik und halbzahlige Quantisierung. *Z. Phys.*, **39**, 828–840.

Li, X., W. Zheng, X. Yang, J. A. Zhang, W. G. Pichel, and Z. Li, 2013: Coexistence of atmospheric gravity waves and boundary layer rolls observed by sar. *Journal of the Atmospheric Sciences*, **70 (11)**, 3448–3459, doi:10.1175/JAS-D-12-0347.1, URL https://doi.org/10.1175/JAS-D-12-0347.1.

Lighthill, M. J., 1978: *Waves in fluids*. Cambridge University Press Cambridge [Eng.] ; New York, xv, 504 p. : pp., URL http://www.loc.gov/catdir/toc/cam027/77008174.html.

Lin, Y., and F. Zhang, 2008: Tracking gravity waves in baroclinic jet-front systems. *Journal of the Atmospheric Sciences*, **65 (7)**, 2402–2415, doi:10.1175/2007JAS2482.1, URL https://doi.org/10.1175/2007JAS2482.1.

Liouville, J., 1836: Sur le développement des fonctions ou parties de fonctions en séries dont les divers termes sont assujettis à satisfaire à une même équation différentielle du second ordre contenant un paramètre variable, I. *J. Math. Pur Appl.*, **1**, 253–265.

Liouville, J., 1837a: Sur le développement des fonctions ou parties de fonctions en séries dont les divers termes sont assujettis à satisfaire à une même équation différentielle du second ordre contenant un paramètre variable, II. *J. Math. Pur Appl.*, **2**, 16–35.

Liouville, J., 1837b: Sur le développement des fonctions ou parties de fonctions en séries dont les divers termes sont assujettis à satisfaire à une même équation différentielle du second ordre contenant un paramètre variable, III. *J. Math. Pur Appl.*, **2**, 418–436.

Liu, C. H., and Coauthors, 1982: Global dynamic responses of the atmosphere to the eruption of mount st. helens on may 18, 1980. *Journal of Geophysical Research: Space Physics*, **87 (A8)**, 6281–6290, doi:10.1029/JA087iA08p06281, URL http://dx.doi.org/10.1029/JA087iA08p06281.

Lognonné, P., 2009: *Seismic Waves from Atmospheric Sources and Atmospheric/Ionospheric Signatures of Seismic Waves*, 281–304. Springer Netherlands, Dordrecht, doi:10.1007/978-1-4020-9508-5_10, URL https://doi.org/10.1007/978-1-4020-9508-5_10.

Lott, F., and C. Millet, 2009: *The Representation of Gravity Waves in Atmospheric General Circulation Models (GCMs)*, 685–699. Springer Netherlands, Dordrecht, doi:10.1007/978-1-4020-9508-5_23, URL http://dx.doi.org/10.1007/978-1-4020-9508-5_23.

Ma, J. Z. G., 2016: Atmospheric layers in response to the propagation of gravity waves under nonisothermal, wind-shear, and dissipative conditions. *Journal of Marine Science and Engineering*, **4 (1)**.

Makela, J. J., and Coauthors, 2011: Imaging and modeling the ionosphere airglow response over hawaii to the tsunami generated by the tohoku earthquake of 11 march 2011. *Geophys. Res. Lett.*, **38**, L00G02, doi:10.1029/2011GL047860, L00G02, doi:10.1029/2011GL047860.

Marks, C. J., and S. D. Eckermann, 1995: A Three-Dimensional Nonhydrostatic Ray-Tracing Model for Gravity Waves: Formulation and Preliminary Results for the Middle Atmosphere. *Journal of Atmospheric Sciences*, **52**, 1959–1984, doi:10.1175/1520-0469(1995)052⟨1959:ATDNRT⟩2.0.CO;2.

Mikumo, T., and S. Watada, 2009: *Acoustic-Gravity Waves from Earthquake Sources*, 263–279. Springer Netherlands, Dordrecht, doi:10.1007/978-1-4020-9508-5_9, URL https://doi.org/10.1007/978-1-4020-9508-5_9.

Muraschko, J., M. D. Fruman, U. Achatz, S. Hickel, and Y. Toledo, 2013: On the application of WKB theory for the simulation of the weakly nonlinear dynamics of gravity waves. *Journal of Atmospheric and Terrestrial Physics*, **90**, 1–25.

Nappo, C. J., 2002: *An Introduction to Atmospheric Gravity Waves*. Academic Press, San Diego, 279 pp.

Nekrasov, A., S. Shalimov, P. Shukla, and L. Stenflo, 1995: Nonlinear disturbances in the ionosphere due to acoustic gravity waves. *Journal of Atmospheric and Terrestrial Physics*, **57 (7)**, 737 – 741, doi:http://dx.doi.org/10.1016/0021-9169(94)00052-P, URL http://www.sciencedirect.com/science/article/pii/002191699400052P.

Nekrasov, A. K., Y. P. Kurchashov, V. N. Ivanov, O. A. Pokhotelov, R. Bharuthram, P. K. Shukla, and L. Stenflo, 1992: Dynamics of density irregularities in the e-region of the ionosphere. *Physica Scripta*, **46 (4)**, 369, URL http://stacks.iop.org/1402-4896/46/i=4/a=011.

Nicholls, M. E., and R. A. Pielke, 1994a: Thermal compression waves. i: Total-energy transfer. *Quarterly Journal of the Royal Meteorological Society*, **120 (516)**, 305–332, doi:10.1002/qj.49712051605, URL http://dx.doi.org/10.1002/qj.49712051605.

Nicholls, M. V. E., and R. A. Pielke, 1994b: Thermal compression waves. ii: Mass adjustment and vertical transfer of total energy. *Quarterly Journal of the Royal Meteorological Society*, **120 (516)**, 333–359, doi:10.1002/qj.49712051606, URL http://dx.doi.org/10.1002/qj.49712051606.

NRLMSISE-00, Community Coordinated Modeling Center, 2016: NRLMSISE-00 Atmosphere Model, http://ccmc.gsfc.nasa.gov/modelweb/models/nrlmsise00.php.

Ostrovsky, L. A., 2008: Ionospheric effects of ground motion: The roles of magnetic field and nonlinearity. *J. Atmos. Sol. Terr. Phys.*, **70**, 1273–1280, doi:10.1016/j.jastp.2008.03.017.

Pokhotelov, O. A., F. Z. Feygin, L. Stenflo, and P. K. Shukla, 1996: Density profile modifications by electromagnetic ion cyclotron wave pressures near the dayside magnetospheric boundary. *Journal of Geophysical Research: Space Physics*, **101 (A5)**, 10 827–10 833, doi:10.1029/96JA00543, URL http://dx.doi.org/10.1029/96JA00543.

Pokhotelov, O. A., V. A. Pilipenko, E. N. Fedorov, L. Stenflo, and P. K. Shukla, 1994: Induced electromagnetic turbulence in the ionosphere and the magnetosphere. *Physica Scripta*, **50 (5)**, 600, URL http://stacks.iop.org/1402-4896/50/i=5/a=026.

Pokhotelov, O. A., D. O. Pokhotelov, F. Z. Feygin, M. Parrot, J. Kangas, K. Mursula, P. K. Shukla, and L. Stenflo, 1998: Excitation of helium cyclotron harmonic waves during quiet magnetic conditions. *Journal of Geophysical Research: Space Physics*, **103 (A11)**, 26 585–26 593, doi:10.1029/98JA02619, URL http://dx.doi.org/10.1029/98JA02619.

Pramitha, M., M. Venkat Ratnam, A. Taori, B. V. Krishna Murthy, D. Pallamraju, and S. Vijaya Bhaskar Rao, 2015: Evidence for tropospheric wind shear excitation of high-phase-speed gravity waves reaching the mesosphere using the ray-tracing technique. *Atmospheric Chemistry & Physics*, **15**, 2709–2721, doi:10.5194/acp-15-2709-2015.

Preusse, P., S. D. Eckermann, and M. Ern, 2008: Transparency of the atmosphere to short horizontal wavelength gravity waves. *Journal of Geophysical Research: Atmospheres*, **113 (D24)**, n/a–n/a, doi:10.1029/2007JD009682, URL http://dx.doi.org/10.1029/2007JD009682, d24104.

Preusse, P., and Coauthors, 2009: Global ray tracing simulations of the saber gravity wave climatology. *Journal of Geophysical Research: Atmospheres*, **114 (D8)**, doi:10.1029/2008JD011214, URL http://dx.doi.org/10.1029/2008JD011214, d08126.

Ratcliffe, J. A., 1962: *The Magneto-ionic theory and its applications to the ionosphere*. University Press, Cambridge, 206 pp.

Rayleigh (John William Strutt), L., 1912: On the propagation of waves through a stratified medium, with special reference to the question of reflection. *Proc. Royal Soc. A*, **86**, 207–226.

ReVelle, D. O., 2009: *Acoustic-Gravity Waves from Impulsive Sources in the Atmosphere*, 305–359. Springer Netherlands, Dordrecht, doi:10.1007/978-1-4020-9508-5_11, URL http://dx.doi.org/10.1007/978-1-4020-9508-5_11.

Rolland, L. M., G. Occhipinti, P. Lognonné, and A. Loevenbruck, 2010: Ionospheric graity waves detected offshore hawaii after tsunamis. *Geophys. Res. Lett.*, **37**, L17101, doi:10.1029/2010GL044479, L17101, doi:10.1029/2010GL044479.

Sato, K., S. Watanabe, Y. Kawatani, Y. Tomikawa, K. Miyazaki, and M. Takahashi, 2009: On the origins of mesospheric gravity waves. *Geophysical Research Letters*, **36 (19)**, doi:10.1029/2009GL039908, URL http://dx.doi.org/10.1029/2009GL039908, l19801.

Schoeberl, M. R., 1985: A ray tracing model of gravity wave propagation and breakdown in the middle atmosphere. *Journal of Geophysical Research: Atmospheres*, **90 (D5)**, 7999–8010, doi:10.1029/JD090iD05p07999, URL http://dx.doi.org/10.1029/JD090iD05p07999.

Smith, M. S., 1975: Phase memory in w.k.b. and phase integral solutions of ionospheric propagation problems. *Proceedings of the Royal Society of London A: Mathematical, Physical and Engineering Sciences*, **346 (1644)**, 59–79, doi:10.1098/rspa.1975.0166, URL http://rspa.royalsocietypublishing.org/content/346/1644/59.

Stenflo, L., 1986: Nonlinear equations for acoustic gravity waves. *Physica Scripta*, **33 (2)**, 156, URL http://stacks.iop.org/1402-4896/33/i=2/a=010.

Stenflo, L., 1987: Acoustic solitary vortices. *The Physics of Fluids*, **30 (10)**, 3297–3299, doi:10.1063/1.866458, URL http://aip.scitation.org/doi/abs/10.1063/1.866458.

Stenflo, L., 1991: Notizen: Acoustic Gravity Vortices in the Atmosphere. *Zeitschrift Naturforschung Teil A*, **46**, 560–560, doi:10.1515/zna-1991-0613.

Stenflo, L., 1996: Nonlinear equations for acoustic gravity waves. *Physics Letters A*, **222 (6)**, 378 – 380, doi:http://dx.doi.org/10.1016/S0375-9601(96)00671-8, URL http://www.sciencedirect.com/science/article/pii/S0375960196006718.

Stenflo, L., and Y. A. Stepanyants, 1995: Acoustic-gravity modons in the atmosphere. *Annales Geophysicae*, **13 (9)**, 973–975, doi:10.1007/s00585-995-0973-3, URL https://doi.org/10.1007/s00585-995-0973-3.

Streltsov, A. V., V. M. Chmyrev, O. A. Pokhotelov, V. A. Marchenko, and L. Stenflo, 1990: The formation and nonlinear evolution of convective cells in the auroral plasma. *Physica Scripta*, **41 (5)**, 686, URL http://stacks.iop.org/1402-4896/41/i=5/a=012.

Suzuki, S., F.-J. Lübken, G. Baumgarten, N. Kaifler, R. Eixmann, B. P. Williams, and T. Nakamura, 2013: Vertical propagation of a mesoscale gravity wave from the lower to the upper atmosphere. *Journal of Atmospheric and Solar-Terrestrial Physics*, **97**, 29 – 36, doi:http://dx.doi.org/10.1016/j.jastp.2013.01.012, URL http://www.sciencedirect.com/science/article/pii/S1364682613000369.

Testud, J., 1970: Gravity waves generated during magnetic substorms. *J. Atmos. Terrest. Phys. 32: 1793-1805(Nov 1970).*, doi:10.1016/0021-9169(70)90137-6.

Tytell, J., F. Vernon, M. Hedlin, C. de Groot Hedlin, J. Reyes, B. Busby, K. Hafner, and J. Eakins, 2016: The USArray transportable array as a platform for weather observation and research. *Bulletin of the American Meteorological Society*, **97 (4)**, 603–619, doi:10.1175/BAMS-D-14-00204.1, URL https://doi.org/10.1175/BAMS-D-14-00204.1.

Uccelini, L. W., 1975: A case study of apparent gravity wave initiation of severe convective storms. *Monthly Weather Review*, **103 (6)**, 497–513, doi:10.1175/1520-0493(1975)103⟨0497:ACSOAG⟩2.0.CO;2, URL https://doi.org/10.1175/1520-0493(1975)103⟨0497:ACSOAG⟩2.0.CO;2.

Vadas, S. L., 2007: Horizontal and vertical propagation and dissipation of gravity waves in the thermosphere from lower atmospheric and thermospheric sources. *Journal of Geophysical Research: Space Physics*, **112 (A6)**, doi:10.1029/2006JA011845, URL http://dx.doi.org/10.1029/2006JA011845, a06305.

Vadas, S. L., and D. C. Fritts, 2005: Thermospheric responses to gravity waves: Influences of increasing viscosity and thermal diffusivity. *Journal of Geophysical Research: Atmospheres*, **110 (D15)**, doi:10.1029/2004JD005574, URL http://dx.doi.org/10.1029/2004JD005574, d15103.

Vadas, S. L., and D. C. Fritts, 2009: Reconstruction of the gravity wave field from convective plumes via ray tracing. *Annales Geophysicae*, **27 (1)**, 147–177, doi:10.5194/angeo-27-147-2009, URL http://www.ann-geophys.net/27/147/2009/.

Vadas, S. L., J. J. Makela, M. J. Nicolls, and R. F. Milliff, 2015: Excitation of gravity waves by ocean surface wave packets: Upward propagation and reconstruction of the thermospheric gravity wave field. *Journal of Geophysical Research: Space Physics*, **120 (11)**, 9748–9780, doi:10.1002/2015JA021430, URL http://dx.doi.org/10.1002/2015JA021430, 2015JA021430.

Volland, H., 1969: The upper atmosphere as a multiply refractive medium for neutral air motions. *Journal of Atmospheric and Terrestrial Physics*, **31**, 491–514, doi:10.1016/0021-9169(69)90002-6.

Šepić, J., I. Vilibić, A. B. Rabinovich, and S. Monserrat, 2015: Widespread tsunami-like waves of 23-27 june in the mediterranean and black seas generated by high-altitude atmospheric forcing. *Scientific Reports*, **5**, 11 682, doi:10.1038/srep11682, URL http://dx.doi.org/10.1038/srep11682.

Weinberg, S., 1962: Eikonal method in magnetohydrodynamics. *Phys Rev.*, **126**, 1899–1909.

Wentzel, G., 1926: Eine Verallgemeinerung der Quantenbedingungen für die Zwecke der Wellenmechanik. *Z. Phys.*, **38**, 518–529.

Williams, B. P., M. A. White, D. A. Krueger, and C. Y. She, 2002: Observation of a large amplitude wave and inversion layer leading to convective instability in the mesopause region over fort collins, co (41n, 105w). *Geophysical Research Letters*, **29 (17)**, 31–1–31–4, doi:10.1029/2001GL014514, URL http://dx.doi.org/10.1029/2001GL014514, 1850.

Wrasse, C. M., and Coauthors, 2006: Mesospheric gravity waves observed near equatorial and low-middle latitude stations: wave characteristics and reverse ray tracing results. *Annales Geophysicae*, **24 (12)**, 3229–3240, doi:10.5194/angeo-24-3229-2006, URL https://www.ann-geophys.net/24/3229/2006/.

Zhang, D.-L., and J. M. Fritsch, 1988: Numerical simulation of the meso-β scale structure and evolution of the 1977 Johnstown Flood. Part III. Internal gravity waves and the squall line. *Journal of the Atmospheric Sciences*, **45 (7)**, 1252–1268, doi:10.1175/1520-0469(1988)045⟨1252:NSOTMS⟩2.0.CO;2, URL https://doi.org/10.1175/1520-0469(1988)045⟨1252:NSOTMS⟩2.0.CO;2.

Zhao, J., and Coauthors, 2017: Lidar observations of stratospheric gravity waves from 2011 to 2015 at McMurdo (77.84°S, 166.69°E), Antarctica: 1. Vertical wavelengths, periods, and frequency and vertical wave number spectra. *Journal of Geophysical Research: Atmospheres*, **122 (10)**, 5041–5062, doi:10.1002/2016JD026368, URL http://dx.doi.org/10.1002/2016JD026368, 2016JD026368.